Bulletin of the Seismological Society of America, Vol. 93, No. 6, pp. 2563–2590, December 2003

Seismic Hazard Maps for Cuba and Surrounding Areas

by Julio García, Dario Slejko, Leonardo Alvarez, Laura Peruzza, and Alessandro Rebez

Abstract A seismic hazard assessment for Cuba and the surrounding areas has been performed in response to a possible revision of the national building code. The hazard assessment has been done according to the standard methodology adopted by the Global Seismic Hazard Assessment Program and by introducing some computational techniques used for the seismic hazard map of Italy. Problems of earthquake catalog treatment, attenuation of peak ground acceleration and macroseismic intensity, as well as seismic source definition have been rigorously analyzed. Thirty-six seismogenic zones have been identified and characterized from a seismicity point of view. The present study offers a picture of the seismic hazard on Cuban territory based on historical seismicity and the benefits drawn from the most recent international investigations on the subject, such as the logic-tree approach used to represent the inevitable uncertainties encountered through the choice of attenuation relation. The final results are maps of the expected shaking with a 475-year return period in terms of peak ground acceleration and macroseismic intensity, which point out the high hazard along the southern coast of Cuba, where the expected ground motion, without the aleatoric uncertainty in the attenuation relations, is between 0.20*g* and 0.30*g*. The rest of the island is characterized by values representing less severe shaking.

Introduction

Cuba is located on the North American plate, north of the boundary with the Caribbean plate, where an approximately sinistral transcurrent motion takes place. The largest earthquakes (Fig. 1) have affected the southernmost part of the island, causing heavy damage in Santiago de Cuba (e.g., the earthquakes of 1578 with magnitude M [corresponding to or calibrated on M_s], 6.75, of 1766 with M 7.5, of 1852 with M 7.3, and of 1932 with M 6.75 [Cotilla, 1998; Chuy, 1999]).

The first attempt to obtain a seismic hazard map of Cuba was based on historical macroseismic data, which have been collected systematically since the early 1960s. A quantitative analysis of the seismological data that took into account the number of events and their recurrence and the maximum intensities reported from 1524 to 1976, including both historical and instrumental data, led to a map of the seismic intensity of Cuba (Chuy and Rodriguez, 1980; revised in Chuy *et al.*, 1983). That study lacked detailed analyses on seismicity and seismogenesis; in addition, no ground-motion attenuation was applied to the intensity data and the maps simply represented the maximum observed shaking.

Seismic hazard estimates for the whole country were computed using the Cornell (1968) probabilistic approach, in McGuire's (1976) formulation, by Rubio (1985). Alvarez and Bune (1985a,b) assessed the seismic hazard for eastern Cuba by using a modified version of the Riznichenko (1979) method to obtain probabilistic estimates with a Poissonian occurrence model. With the same methodology, Alvarez *et al.* (1991) undertook a new study devoted to the whole Cuban region in terms of macroseismic intensity, published in the *Nuevo Atlas Nacional de Cuba* (1989). There, attenuation was considered by the elliptical isoseismal model proposed by Alvarez and Chuy (1985).

For the present Cuban building code, Chuy and Alvarez (1995) presented a map that shows the horizontal peak ground acceleration (PGA) with an 85% nonexceedence probability in 50 years for an average soil (without classification of the site geology); the PGA was calculated from macroseismic intensity using the Trifunac and Brady (1975) relationship. The Chuy and Alvarez (1995) map was constructed from the results by Orbera *et al.* (1990), Chuy *et al.* (1992), and Gonzalez *et al.* (1993), for different regions of Cuba. This decision caused a nonuniform treatment of the information, as the basic works did not use the same methodology.

More recently, probabilistic seismic hazard estimates for the whole of Cuba were prepared by Rodriguez *et al.* (1997) in terms of macroseismic intensity, then translated into PGA. They employed the Cornell (1968) approach, in the McGuire (1976) formulation, using the computer program SACUDIDA (Alvarez, 1995). The results were presented as a set of curves and maps, and the estimates ob-

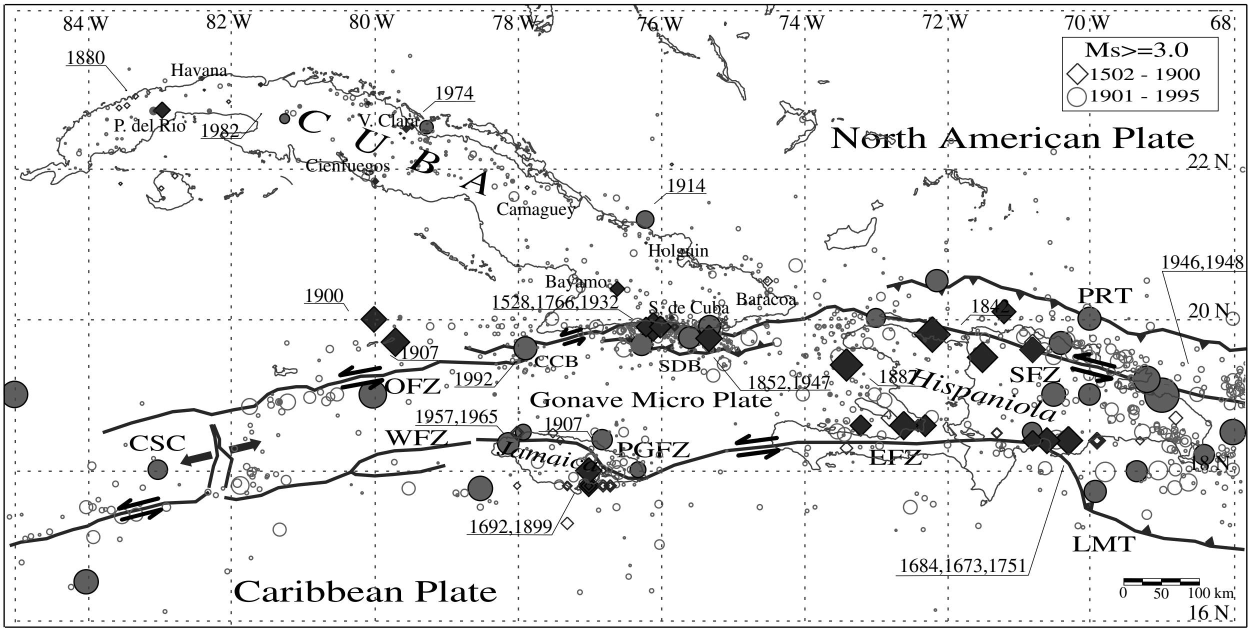

Figure 1. Independent earthquakes (1502–1995, $M_s \geq 3$) in the vicinity of Cuba: diamonds indicate historical events (pre-1900), circles show events of the twentieth century, and solid symbols pinpoint the most important earthquakes. The major faults are indicated with the following abbreviations: CSC, Cayman spreading center; WFZ, Walton fault zone; OFZ, Oriente fault zone; PGFZ, Plantain Garden fault zone; EFZ, Enriquillo fault zone; SFZ, Septentrional fault zone; PRT, Puerto Rico trench; LMT, Los Muertos trench; CCB, Cabo Cruz basin; SDB, Santiago deformed belt.

tained were lower than the previously obtained ones in the western region and similar in the east-central zone.

In the context of the International Decade for Natural Disasters Reduction, the Global Seismic Hazard Assessment Program (GSHAP) (Giardini and Basham, 1993; Giardini, 1999) implemented a regionalized strategy for the assessment of seismic hazard based on a mosaic of multinational test areas and regions. In the GSHAP project, the results by Shepherd *et al.* (1997) for the Caribbean, based on the historical parametric method (Veneziano *et al.*, 1984), were taken and inserted into the hazard map of North and Central America (Shedlock, 1999; Shedlock and Tanner, 1999). The results can be considered preliminary, as the applied method (Veneziano *et al.*, 1984) used incomplete data and information about Cuban seismicity.

Our general comments on the state of the art of seismic hazard assessment for Cuba are as follows:

- Estimates for both the central and the western regions of the island show a certain degree of subjectivity due to the scarcity of events in some seismicity zones;
- Source zonation is a problem not yet resolved, as each map (Alvarez *et al.*, 1991; Chuy and Alvarez, 1995; Rodriguez *et al.*, 1997) presents only a partial view of the seismotectonics of the area and not within a general kinematic framework;
- The use of ground-motion parameter values (PGA, velocity, or displacement) computed from intensity (Trifunac and Brady, 1975), instead of using proper attenuation relations, makes the calculated hazard in terms of those parameters less reliable.

The aim of the present study is to propose new probabilistic seismic hazard estimates for the Cuban territory and the surrounding region (the islands of Jamaica and Hispaniola), using a standard probabilistic approach (Cornell, 1968) and importing some of the procedures adopted by other nations dealing with the problem of revising and updating their national building codes. The present work benefits from the Italian experience matured in the Gruppo Nazionale per la Difesa dai Terremoti activities (Slejko *et al.*, 1998) and applied to the GSHAP test area ADRIA (Slejko *et al.*, 1999), a project that involved many European countries. Estimates in terms of PGA and macroseismic intensity have been considered; the computation was done by the computer code SEISRISK III (Bender and Perkins, 1987), and a complete revision of the attenuation relationships for macroseismic intensity is proposed here. In order to represent the uncertainties produced by the choice of the attenuation relation adopted, the logic-tree methodology has been applied.

Seismicity

Documented Cuban seismic history began in the sixteenth century, when several great earthquakes (Chuy *et al.*, 1983) occurred in the Greater Antilles (Cuba, Jamaica, Hispaniola, and Puero Rico) (see Fig. 1). The city of Santiago de Cuba, in the southeastern part of the island, was partially destroyed by some of these strong earthquakes: according to Chuy (1999), they happened in 1766 and 1852, when the maximum observed intensity (I_{max}) reached IX Medvedev–Sponheuer–Karnik (MSK) (Sponheuer, 1960). The MSK intensity scale is similar to the modified Mercalli scale (Richter, 1958) with the main differences related to weak ground shaking (Fig. 2) (Murphy and O'Brian, 1977). The remaining territory has been affected by less frequent intraplate seismicity associated with minor tectonic structures, and during the documented period only one earthquake (the 1880 San Cristobal–Candelaria earthquake, I_{max} = VIII MSK) occurred in the northwestern part of the island, causing damage similar to that described for Santiago de Cuba.

Seismological Data Collection and Earthquake Catalog

Several kinds of data are available for Cuba and the neighboring regions: macroseismic for the sixteenth to nineteenth and part of the twentieth centuries (Chuy, 1999), instrumental from international seismological agencies (International Seismological Centre [ISC] and U.S. Geological Survey [USGS]) during the twentieth century, and instrumental from the Cuban local network since 1964 (Servicio Sismológico Nacional, 1964–1995).

For systematic storage and processing of data to be used in the present hazard assessment, we decided to create a new database where each earthquake could be characterized by several entries, one for each source of information available. The database was prepared by merging all previously cited data sources (British Association Seismology Committee, 1918, 1919, 1921; International Seismological Summary, 1918–1963; ISC, 1964–1995; Preliminary Determination of Epicenters, 1968–1995; Servicio Sismológico Nacional, 1964–1995; Chuy, 1999). This main data set was used to prepare a catalog characterized by only one entry for each event, selecting the most reliable data. This selection was done in two steps, the first with the aid of the computer program EDCAT (Gabrielov *et al.*, 1986), which allowed us to discard the evident duplicated entries, the second by visual checking of the data set. The final catalog contains 9241 earthquakes from 1502 to 1995 (Table 1), which describes Cuban seismicity better than the GSHAP catalog (Tanner and Shepherd, 1997; Shedlock, 1999). For our study area, the Tanner and Shepherd (1997) catalog contains only 15% of the events of the catalog used in this study for the period before 1900 and 25% after that. Most of the events of our new catalog have an estimate of magnitude (Table 2). In the case of macroseismic data, the magnitude M_I was taken from Chuy (1999), who computed M_I by fitting the isoseismals according to the Fedotov and Shumilina (1971) attenuation model:

$$M_I = 0.6667 I_S + 1.7533 \log r + 0.0058 r - 1.6667, \quad (1)$$

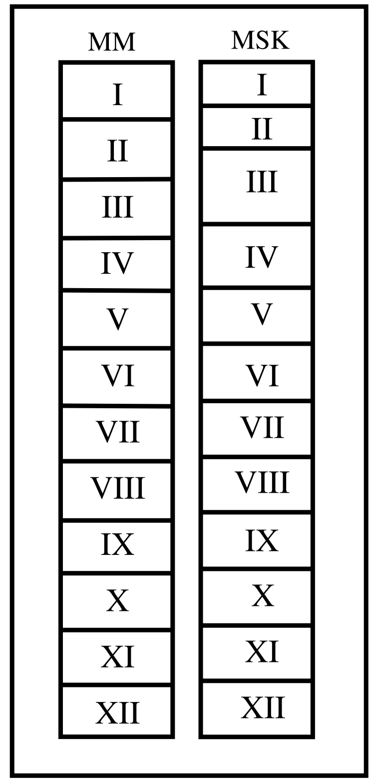

Figure 2. Comparison between the modified Mercalli (MM) and Medvedev–Sponheuer–Karnik (MSK) macroseismic scales (from Murphy and O'Brian, 1977).

Table 1
General Characteristics of the Earthquake Catalog

Time window	1502 to 30 December 1995
Latitude range	16.00°–24.00° N
Longitude range	67.00°–86.00° W
Depth range (km)	0–300
Intensity range (MSK)	II–X

Table 2
Quantification of Earthquake Size in the Catalog

Reported Magnitude	Events	%	Interval
M_s	289	3.13	1.4–8.1
M_I	1045	11.31	2.0–8.2
m_b	411	4.45	2.2–6.7
M_l	137	1.48	1.8–7.1
Ms_D	1122	12.14	0.1–6.7
Ms_{KD}	2953	31.96	0.1–6.6
Ms_{KR}	2456	26.58	0.4–5.8
Without M	829	8.97	—
M (total)	9241	100.00	0.1–8.2

M_s and m_b refer to surface and body wave magnitudes, M_L is the local magnitude coming from international agencies, and M_I represents the magnitude obtained by macroseismic data inversion. Ms_D, Ms_{KD}, and Ms_{KR} refer to the surface-wave magnitude obtained by the Alvarez *et al.* (1990) regression relationships (equations 4, 5, and 6, respectively).

where I_S is the intensity at the study site and r is its epicentral distance.

The size of the recent earthquakes recorded by the Cuban seismographic network is given in the bulletins by two energetic parameters, K_r and K_D (Rautian, 1964; Alvarez *et al.*, 1990):

$$K_r = 1.8 \log [(A_P + A_S)/2] + 2.1 \log (8\ T_{SP}) + 0.7 \quad (2)$$

$$K_D = 4.7 \log D - 1.2, \quad (3)$$

where A_P and A_S are the maximum amplitudes of the P and S waves, respectively, T_{SP} is the interval between the P- and S-wave arrival times, and D is the total duration of the recording.

M_s was computed by the Alvarez *et al.* (1990) formulae:

$$M_s = 3.2 \log D - 4.5 \quad (4)$$

$$M_s = 0.68\ K_D - 3.68 \quad (5)$$

$$M_s = 0.48\ K_r - 1.5\ . \quad (6)$$

A new relation to compute M_s from m_b, valid in the interval $4.0 < m_b < 6.0$ and $3.1 < M_s < 6.7$, was obtained by linear regression and used (see Garcia [2001] for details)

$$M_s = 1.37\ m_b - 2.34\ . \quad (7)$$

No substantial difference was recognized between M_s, M_I, and M_L, as both M_I and M_L were originally calibrated on M_s data.

The most common hypothesis in probabilistic seismic hazard assessment is that the earthquake occurrences form a Poisson process, that is, a process stationary in time of independent and nonmultiple events. With this in mind, it is necessary to identify, as clearly as possible, the foreshocks and aftershocks and to eliminate them from the catalog in order to work only with a catalog of the mainshocks that can be considered independent.

In the Gardner and Knopoff (1974) declustering approach, an event is considered an aftershock if (1) its magnitude does not exceed that of the mainshock, (2) the distance between its epicenter and that of the mainshock is smaller than $L(M)$, and (3) the difference between its origin time and that of the mainshock is smaller than $T(M)$, where $T(M)$ and $L(M)$ are empirical functions of magnitude M:

$$\log T(M) = a_1 M + b_1 \quad (8)$$

$$\log L(M) = a_2 M + b_2 . \quad (9)$$

We identified 35 seismic sequences in the Greater Antilles (main events in the M 3–8 range) and computed, by visual evaluation, the distance $L(M)_i$ between the main event and the farthest aftershock and the time interval $T(M)_i$ between the main event and the last aftershock, for each i of the 35 studied sequences. Contrary to Gardner and Knopoff (1974), who took the envelope of the maximum $T(M)_i$'s and $L(M)_i$'s only, we removed all $T(M)_i$'s and $L(M)_i$'s largely below their average populations (open symbols in Fig. 3) and computed the a_i and b_i ($i = 1,2$) coefficients in equations (8) and (9) by linear regression. The reason we followed this approach is that most events do not have a well-constrained location and, therefore, it seemed reasonable to average the data.

As shown on Figure 3, our $T(M)_i$ values are lower than those given by Gardner and Knopoff (1974) for California, while the $L(M)_i$ values are similar to those obtained by Gardner and Knopoff (1974) for events larger than M 6. Below that magnitude, our values show a great dispersion, because there is no uniformity in the event detection for the entire region, it being better in southeastern Cuba. In fact, weak ($M < 3.0$) aftershocks in south Jamaica or Hispaniola are missing in our catalog because they were not reported by international agencies, such USGS or ISC, while the recent southeastern Cuban earthquakes were well documented. For the period preceding the installation of stations on the Cuban territory (i.e., before 1968), when most of the information is macroseismic or a mixture of instrumental and macroseismic data, it was necessary to pay special attention to the epicentral data. In fact, some events offshore Cuba have the epicentral coordinates of the mainshock computed instrumentally, while the aftershock coordinates are associated to the inland location with the highest macroseismic intensity. The $L(M)$ value in these cases is very uncertain and was not used in our elaborations.

As can be seen in Figure 3 the data for Jamaica, Hispaniola, and Puerto Rico are almost always lower than those for Cuba: two separate regressions were then computed. The obtained values of the parameters in equations (8) and (9) and the correlation coefficient R are $a_1 = 0.41$ and $b_1 = -0.40$ with $R = 0.99$ and $a_2 = 0.36$ and $b_2 = 0.21$ with $R = 0.90$ for Cuba and $a_1 = 0.17$ and $b_1 = 0.86$ with $R = 0.75$ and $a_2 = 0.09$ and $b_2 = 1.08$ with $R = 0.67$ for Jamaica, Hispaniola, and Puerto Rico.

After the removal of all outliers from the population of the maxima for each magnitude class [data with short $T(M)$ or $L(M)$ with respect to their magnitude], the data [both $T(M)_i$'s and $L(M)_i$'s] referring to Jamaica, Hispaniola, and Puerto Rico also show a large dispersion. Because the relative fit is not well constrained, it was decided to use the *a*- and *b*-values calculated for Cuba for the whole study region. A data set of 6733 independent events with magnitude determination was obtained, which is judged suitable for hazard assessment.

The time distribution of the seismicity in the study region is presented in Figure 4. The occurrence of large-magnitude ($M \geq 7$) events with a recurrence of about 100 years can be clearly seen (Fig. 4a). From 1900, the number of small- and moderate-magnitude ($3 < M < 6$) earthquakes

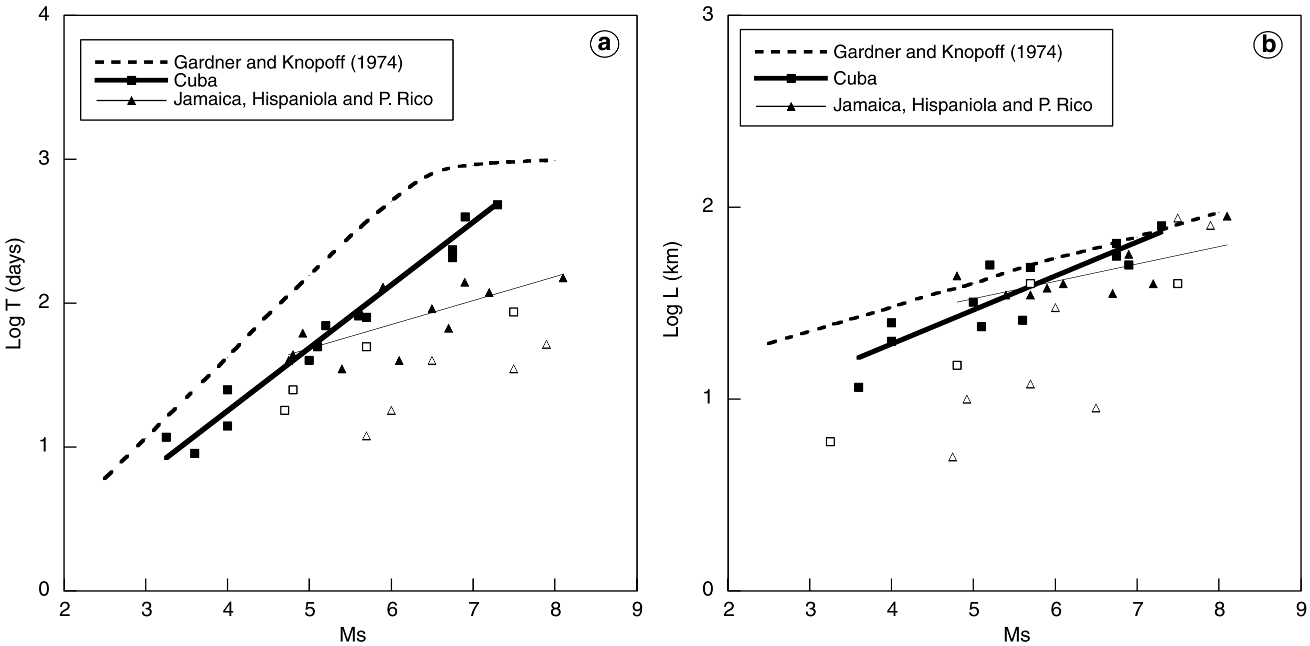

Figure 3. Time (a) and space (b) declustering: two different relations are computed, respectively, for Cuban earthquakes (squares) and earthquakes on the other islands (triangles). Open symbols indicate data not used in the regressions. The dashed lines show the Gardner and Knopoff (1974) relations.

increases, but a sort of small gap can be seen between 1910 and 1930, soon before the occurrence of the large earthquake in 1932 (M_s 6.75) offshore Santiago de Cuba (Fig. 4b). The period 1900–1970 represents a very seismically active interval, while no large earthquakes have occurred recently.

Spatial Characteristics of the Regional Seismicity

The Caribbean seismotectonics are governed by the interaction of the Caribbean plate with the North American plate. The Caribbean–North American plate boundary zone (Fig. 1) comprises the Polochic–Motagua and the Swam Islands fault zones (not presented in Fig. 1) and the mid-Cayman spreading center (CSC). Eastward, the plate boundary splays into two branches: The northern one consists of the upper extremity of the CSC, the Oriente fault zone (OFZ), the Septentrional fault zone (SFZ), and the "19° fault" (Speed and Larue, 1991); this last one is located on the northern Puerto Rico margin (outside Fig. 1). The southern branch begins at the lower end of the CSC and comprises the Walton fault zone (WFZ), the Enriquillo fault zone (EFZ), the Plantain Garden fault zone (PGFZ), the Muertos Trough, and the Anegada Passage fault zone. Both branches meet each other to the east, in the Lesser Antilles subduction zone. The eastward motion of the Caribbean plate produces left-lateral deformation (Moreno *et al.*, 2002) along the EFZ, the WFZ, and the OFZ.

The northeastern Caribbean plate is characterized by complex tectonics, with several subduction zones. Different authors have hinted at the existence of several microplates in the eastern Caribbean: Rozencrantz and Mann (1991) identified the region delimited by the OFZ, the WFZ, and the EFZ/PGFZ as one of them, and they named it the Gonave Microplate.

The seismicity in the vicinity of Cuba (Fig. 1) clearly indicates the capability of the boundary between the North American and Caribbean plates to produce strong events: from the CSC, which generates normal-faulting earthquakes, to the OFZ and the SFZ, where very large transpressive and strike-slip earthquakes have occurred. South of the OFZ, the southern edge of the plate boundary zone is defined by the left-lateral strike-slip WFZ, where some large events have been reported near Kingston City.

Cuban seismicity can be divided into two types (Alvarez *et al.*, 1991): intraplate and interplate. Interplate seismicity affects the southeastern region, where the earthquakes occur mainly in the OFZ. The first historical earthquake was reported at Baracoa, the first villa founded in Cuba by the Spaniards in 1511, located on the northern coast of eastern Cuba. Seismic activity in southern Cuba is located along the coast and mainly offshore. The strongest concentration of seismicity can be seen around Santiago de Cuba, where the largest earthquakes in Cuba were felt (1766 and 1852, both with I_{max} = IX MSK). The intraplate seismicity affects the rest of the country, the events occurring in the vicinity of some tectonic structures (e.g., Pinar and La Trocha faults; see Fig. 5). During the documented period only one earthquake causing strong damage (the 1880 San Cristobal–Candelaria earthquake, M 6.0 and I_{max} = VIII MSK) occurred in the Pinar del Rio region (northwestern Cuba).

Small- to moderate-magnitude seismicity, recorded by

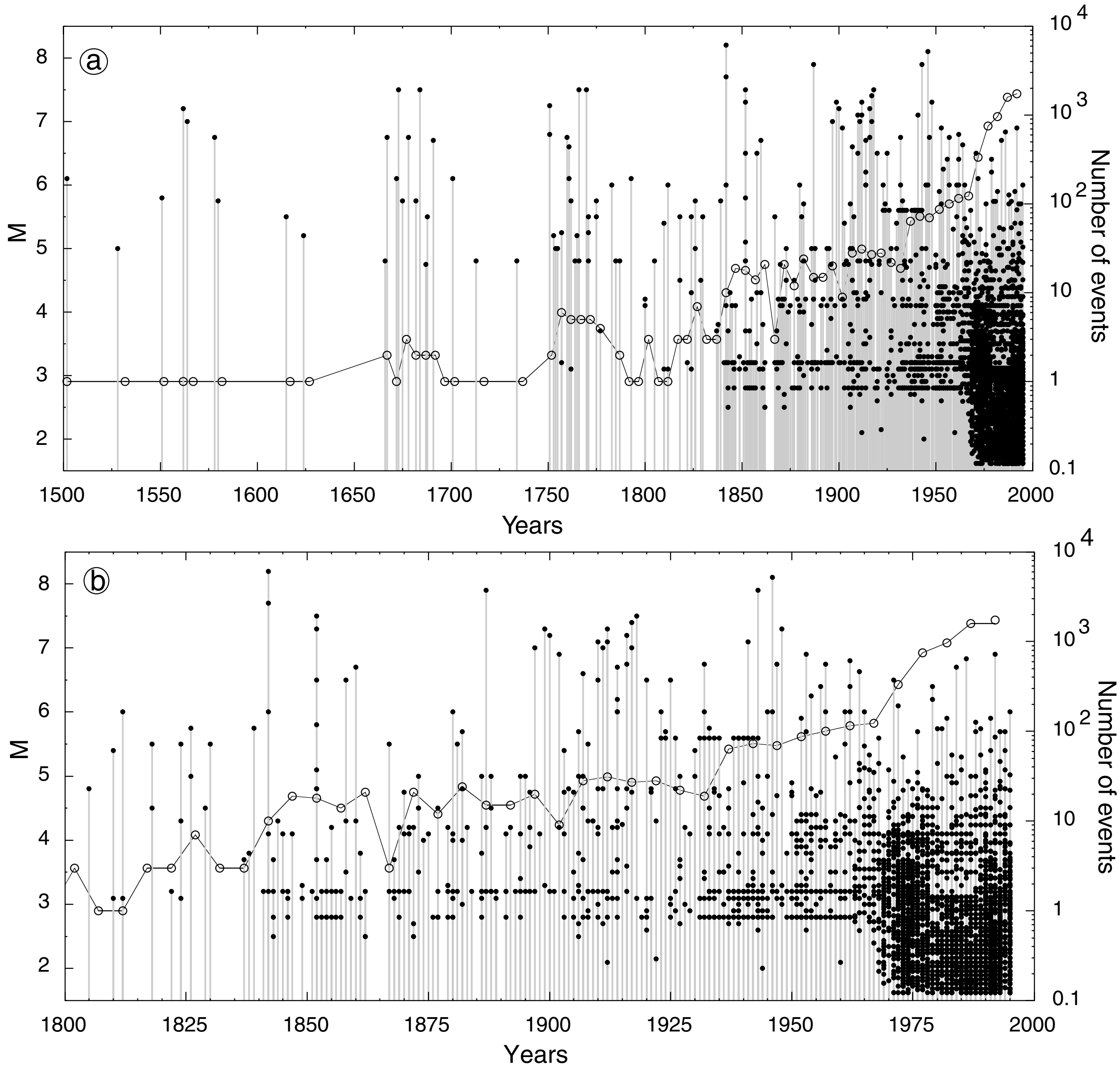

Figure 4. Time distribution of seismicity for the study region: (a) time period 1500–1995, (b) time period 1800–1995. The solid dots indicate the magnitude of the earthquakes. The open dots represent the number of events in 5 years.

the Cuban National Network, is located in the eastern region, and some events have occurred in the westernmost part of the island, such as those of December 1982 (I_{max} = VI MSK; M_s 4.9) and March 1995 (I_{max} = V) (MSK, M_s 2.5).

Seismotectonics and Seismogenic Zoning for Cuba

According to Iturralde-Vinent (1996), Cuba consists of two separate geological units: a foldbelt and a neoautochthon. The foldbelt can be subdivided into continental units and oceanic units. The continental units comprise the Mesozoic Bahamian platform and slope deposits, which are overlaid by a Paleocene–Late Eocene foreland basin, and the Cuban Southwestern Terranes, which were probably originally attached to the Yucatan Platform. The oceanic units are the northern ophiolite belt, the Cretaceous volcanic arc, which is overlaid by the latest Cretaceous–Late Eocene piggyback basins, and the Paleocene Middle–latest Eocene piggyback basin. The neoautochthon encompasses latest Eocene to Holocene slightly deformed sedimentary rocks, which represent the true evolution of Cuba up to its present-day shape.

Seismotectonic studies in Cuba started during the 1970s (Belousov *et al.*, 1983) with a methodology based on the representation of the neotectonic history of the study region

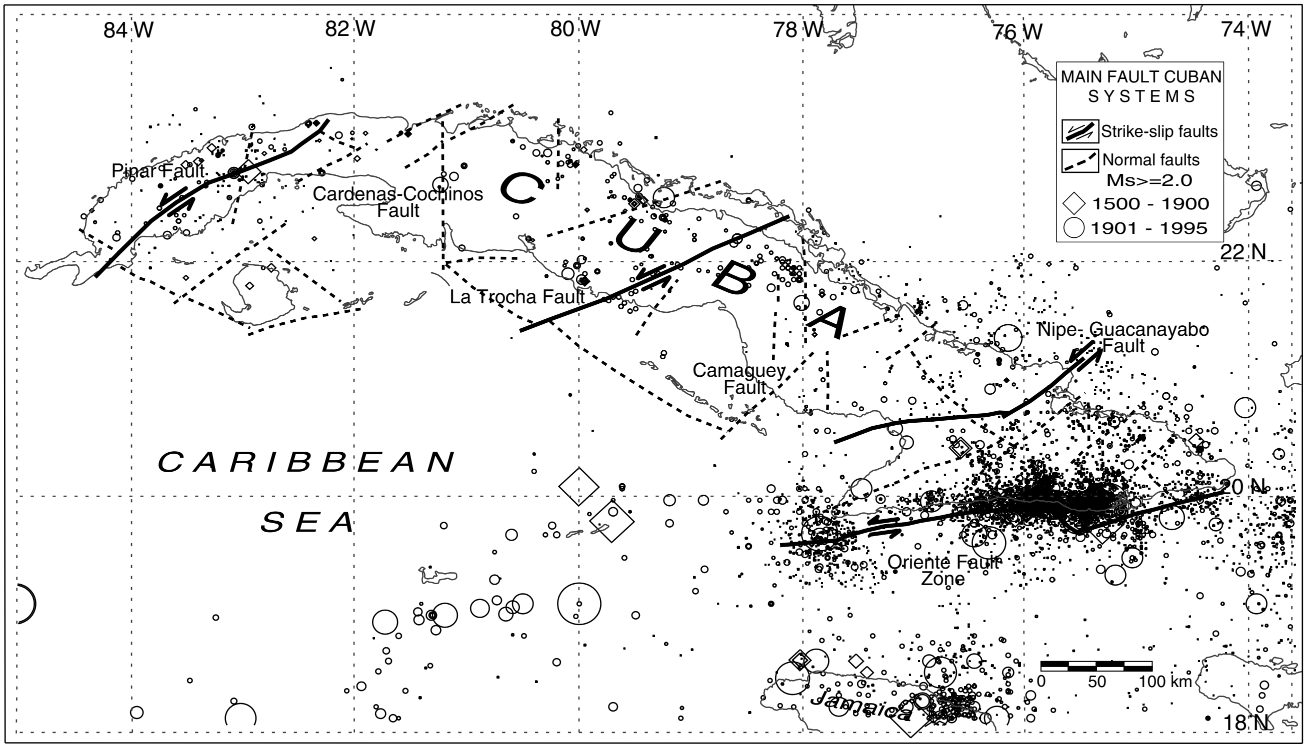

Figure 5. Map of the principal faults in Cuba (modified from Iturralde-Vinent, 1996). Solid lines show strike-slip faults; dashed lines represent normal faults. The epicenters of earthquakes (diamond, pre-1900; circles, during the twentieth century) with magnitude larger than, or equal to, 2 are reported.

widely applied in the former Soviet Union: the amplitudes and velocities of vertical movements in the Neogene–Quaternary, Pliocene, and Holocene are associated with the fault systems, and the seismogenic zones (SZs) are evaluated according to their morphological and seismological characteristics.

In eastern Cuba, various local studies have been made since then. All of them used the same methodology proposed by Belousov *et al.* (1983) or combined it with other geophysical results (Orbera *et al.*, 1989, 1990).

Cotilla *et al.* (1991) prepared a seismotectonic map on the basis of plate tectonic theory. The delineation of the SZs was based on the main alignments from remote sensing, integrated with the results obtained from geology, neotectonics, geophysics, and seismicity. This approach considered the possibility of earthquake occurrences on blind faults for the first time.

The differences between the Cotilla *et al.* (1991) map and those prepared previously, and used by Chuy and Alvarez (1995) for hazard computation, are mainly in the definition of minor SZs and their maximum magnitude. While Cotilla *et al.* (1991) eliminated some SZs (whose seismicity is treated as background seismicity), Chuy and Alvarez (1995) decided to consider all the SZs known, assuming that those with similar seismicity, seismotectonic conditions, and maximum magnitude can be combined.

Seismogenic Zonation for Hazard Purposes

Without a complete instrumental data set over a significant time period and detailed geological investigations devoted to recognizing possible seismogenic sources, it is difficult to improve our seismotectonic knowledge. Knowledge of crustal kinematics can help, and some methodological examples do exist (e.g., Meletti *et al.*, 2000) where the seismogenic zonation is based on an adequate kinematic model in which there must exist a logical link between the areas under stress conditions and the balance of space (the consumed one has to be compensated by the created one), under some established boundary conditions.

Taking into account the complexity of the Cuban tectonic environment (Iturralde-Vinent, 1996), the poor knowledge about the kinematic evolution of the principal fault systems, and the uncertainty in the hypocentral location of historical events (uncertainty of 15–20 km or more in the horizontal coordinates is reasonable), it is impossible to associate earthquakes with individual faults. This fact is even more relevant in an intraplate region like Cuba, where, for some zones, both geology and tectonics are better known than seismicity, due to the scarcity of large earthquakes.

In regions where the seismicity is low or poorly documented (this is the case for the intraplate Cuban region), the geological and tectonic information, described hereafter, is very important to identify the seismic sources (especially those with a long return period) that can produce future earthquakes and, therefore, contribute to seismic hazard.

The basis of the present seismogenic zonation is the map proposed by Cotilla *et al.* (1991), also recently used by Rodriguez *et al.* (1997). It was modified during the present study for a more robust application of the seismotectonic probabilism approach (Muir-Wood, 1993) with the following criteria:

- Each SZ must contain enough earthquakes to construct a magnitude–frequency graph;
- Considering the selected scale of the work (1:1,000,000), short or long faults, only a few kilometers apart, were grouped together.

The seismogenic zonation obtained consists of 36 SZs (Fig. 6), where each SZ represents the surficial projection of one or more seismogenic structures having similar behavior and rupture mechanism. Three main SZ classes are identified: (1) SZs with a dominant left-lateral (transpressive) faulting, probably related to the northern margin of the Caribbean plate (SZ25–SZ36); (2) SZs with mainly vertical movements (SZ1–SZ7, SZ10, SZ11, SZ13–SZ15, SZ18, and SZ20–SZ24); and (3) SZs with pre-Eocene faults roughly parallel to the OFZ, with a less than 50-km left-lateral wrench displacement and minor deformation along very narrow stripes (SZ8, SZ9, SZ12, SZ16, SZ17, and SZ19).

Uncertainties in SZ location are taken into account and used later in the computation of seismic hazard (this is one of the advantages of the code SEISRISK III [Bender and Perkins, 1987]), as most of the SZs are adjacent polygons. The boundary variation is applied inward, leaving a source of similar shape but smaller in size. In Figure 6, the SZ border uncertainties are marked with a symbol after the SZ name and gray areas indicate the intensity attenuation relationship for the SZ. The seismicity that remains outside the proposed zonation has been collected into three wide background zones for hazard computation.

The 36 SZs are grouped into 19 seismic regions from the tectonic point of view, which are briefly described in the following.

Seismic Region Norte Cubana (SZ1–SZ6). These SZs represent segments of the North Cuban fault (NCF), which extends for more than 1000 km along the whole north coast of the island. Vertical displacements as large as 300 m are documented in many transverse seismic profiles along the Cuban north slope (Orbera *et al.*, 1990). The structure is presented in the form of blocks displaced by faults with a southwest–northeast Cayman direction. This structure constitutes the limit of the interplate tectonic system, presenting a significant contrast between the northeastern border of the Cuban megablocks and the submarine depression of suture of the Old Channel of the Bahamas. The seismicity is concentrated at the intersection of the NCF with the major southwest–northeast–oriented faults that cut it.

Seismic Region Consolacion del Norte (SZ7). The Consolación del Norte fault is a deep fault of regional character,

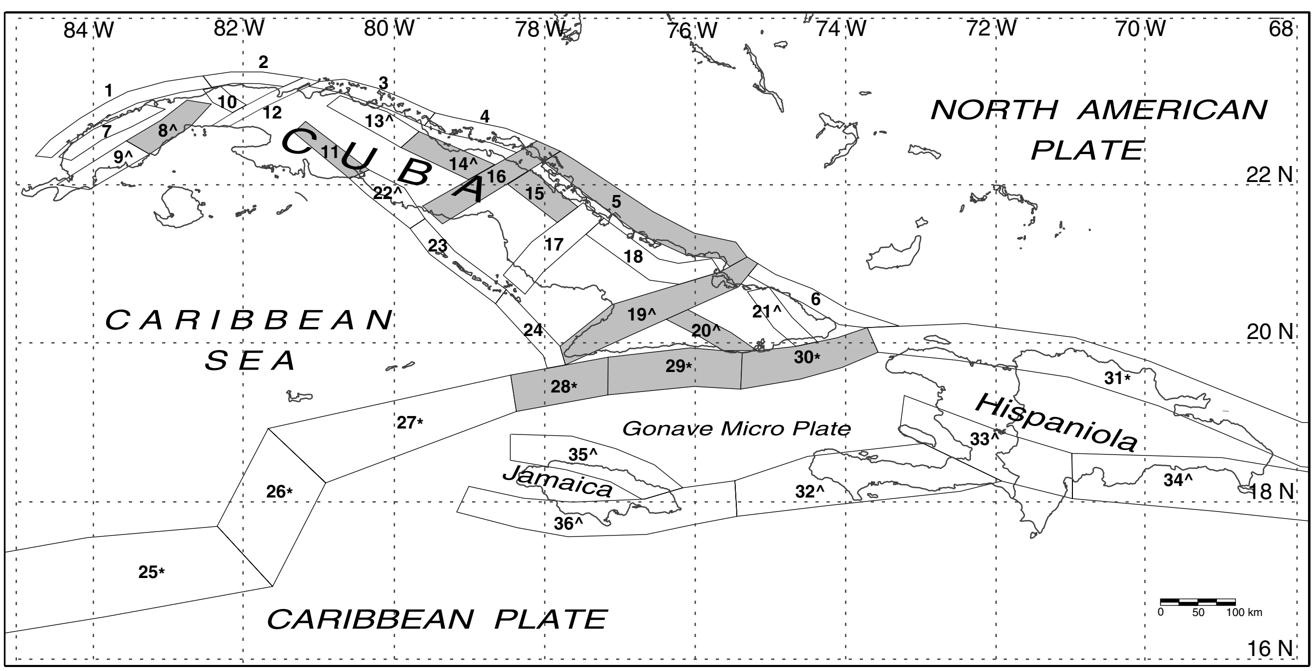

Figure 6. SZs in the vicinity of Cuba. The numbers indicate the SZ code. The symbol after the numbers represents the border uncertainty introduced in the seismic hazard computation: *, 15–20 km, ∧, 5–10 km; none, 1 km. Gray SZs indicate that an individual intensity attenuation relationship was used.

with recent seismicity. It has an extension of 115 km and an average depth of 25 km.

Seismic Region Pinar (SZ8, SZ9). The Pinar faults constitute a system whose planes dip to the south, submerging under a 3-km-thick layer of Neogene–Quaternary silts (Pucharovsky *et al.*, 1989). It is the most important fault system in western Cuba, with a length of 180 km approximately in the southwest–northeast direction, a depth of 25 km, and a width of 5 km (Pucharovsky *et al.*, 1989; Iturralde-Vinent, 1994). It can be clearly observed from satellite images (Orbera *et al.*, 1990; Cotilla *et al.*, 1991) with a vertical displacement of around 2000 m in the Neogene–Quaternary terrains. According to the geological data (Pucharovsky *et al.*, 1989), its development initiated in the preorogenic stage and was reactivated in the Neogene–Quaternary. The most intense movements (more than 3 km) took place in SZ8, where the M 6.0 22 January 1880 earthquake (VIII MSK in San Cristobal and Candelaria) occurred.

Seismic Region Havana (SZ10). This region is associated with the fault system with the same name, which has an approximate extension of 100 km and a total neotectonic displacement of 0.2 km (Orbera *et al.*, 1989). Although the earthquakes reported in Havana and some locations of its province cannot be attributed to the western portion of the Norte Cubana seismic region, the seismic activity of the Havana fault system is still under debate.

Seismic Region Jagüey–Cienfuegos (SZ11). Although it coincides with a deep fault located under younger tectonic sequences, it does not have a well-defined character. The earthquakes in the Torriente–Jagüey Grande and Cienfuegos Bay areas can be associated with this fault, as well as the 9 March 1995 earthquake in San José de las Lajas (Cotilla and Alvarez, 2001).

Seismic Region Hicacos (SZ12). It is associated with a deep fault (Iturralde-Vinent, 1994) above Paleocene–Quaternary formations, splitting the ophiolities sequence that makes the main Cuban watershed deviate abruptly, causing different types of fluvial networks. The earthquakes reported in Matanzas and more recently in the Varadero–Cardenas area are associated with this structure.

Seismic Region Las Villas (SZ13, SZ14). Associated with a deep fault that divides the younger coastal formations of the north from the older ones of the south, it appears as a negative anomaly in the gravimetric map (Cuevas, 1994) and with positive and negative anomalies in the magnetic field. Medium-magnitude seismicity is associated with this fault.

Seismic Region Trocha (SZ16). This structure is associated with a deep fault more than 180 km long, with neotectonic transcurrent activity, documented by geological data (Iturralde-Vinent, 1996), which represents the limit of the central Cuban basin. It constitutes an area of anomalous gradients of the geophysical fields with negative values (Gonzalez *et al.*, 1993). Its seismicity is documented by the earthquakes reported in the Santi Spiritus region.

Seismic Region Camagüey (SZ17). Associated with a regional transverse fault with lateral displacement that affects the whole crust and constitutes the boundary between two megablocks, this deep fault, which cuts young as well as old sequences, is 140 km long and intersects the Cubitas fault. Consequently, the earthquakes in Camagüey and Vertientes are associated with it. The gravimetric and magnetic fields show apparent inflections (Gonzalez *et al.*, 1993; Cuevas, 1994).

Seismic Region Cubitas (SZ15, SZ18). It is associated with a northwest–southeast–oriented deep fault that constitutes a portion of the Cuban marginal suture and is considered to be the main structure in central Cuba. It is cut by the Camagüey and the Trocha traverse faults, where seismicity is documented. The 1974 Esmeralda earthquake (M_s 4.5, I_{max} = VII MSK) is linked to this zone as well.

Seismic Region Cauto–Nipe (SZ19). This structure is associated with a southwest–northeast–oriented fault system, where the Nipe–Guacanayabo and Cauto Norte faults are the principal ones. The latter is, according to the geophysical data, a 210-km-long and 30-km-deep fault. The most significant earthquakes occurred in Bayamo in 1551 (VIII MSK), 1624 (VII MSK), and 1987 and 1988 (both V MSK).

Seismic Region Baconao (SZ20). It is associated with a fault that is better defined in its eastern part, where it has a clear expression mainly in relief and significant seismic activity at the intersection with the Bartlett–Cayman fault (SZ29 and SZ30).

Seismic Region Purial (SZ21). This seismic region is associated with deep strike-slip faults that do not have a clear expression on the relief, but are pinpointed very well in the gravimetric map (Chuy *et al.*, 1992; Cuevas, 1994). The epicenters of small-magnitude ($M \leq 3$) events are aligned along the fault.

Seismic Region Sur-Cubana (SZ22–SZ24). The Sur-Cubana seismic region is associated with new deep faults that extend for over 300 km all along the major part of the Cuban southern coast. Only moderate ($M < 5$, $I_{max} \leq$ VI MSK) earthquakes occurred there in the past.

Seismic Region Swan Islands (SZ25). It is associated with a strike-slip fault evidenced by recent marine geophysical studies (Lundren and Russo, 1996), with the exception of one small part of overstepping splays, according to Rosencrantz and Mann (1991).

Seismic Region Cayman Spreading Center (SZ26, SZ27). This region is characterized by earthquakes associated with normal faults and magnetic anomalies in the Cayman Trough (Rosencrantz *et al.*, 1988). The northern end of the CSC terminates against the OFZ. Here, seismicity is caused by a pure left-lateral strike-slip motion.

Seismic Region Oriente (SZ28–SZ30). It is associated with the Bartlett–Cayman fault system, which is more than 1600 km long, 50 to 100 km wide, and more than 50 km deep. It presents a predominant east–west direction and constitutes the southern limit of the North American plate, to which Cuba belongs. This structure also constitutes a limit of morphostructures of the global tectonic system and presents a notable topographical contrast (+8000 m) between the megablocks of the crests and valleys of Cayman (Calais *et al.*, 1991). The high neotectonic activity of this region was documented by Lundgren and Russo (1996); the highest level of seismicity of the whole of Cuba occurs in this area. In fact, 22 out of 28 catastrophic earthquakes in the Cuban archipelago have occurred here, 20 of them in the Santiago de Cuba area (M_s 7.6 in 1766 and M_s 7.3 in 1852, both with IX MSK) and two in the Cabo Cruz–Pilon area. In the Pilon area, the strongest earthquake happened on 25 May 1992 (M 6.8), producing a VII MSK intensity. More than 3000 small to moderate ($M < 5$) earthquakes have been recorded during the last 20 years.

Seismic Region Hispaniola (SZ31–SZ34). Several faults are active in a restraining bend in its northern part (SZ31) (Mann *et al.*, 1984; Russo and Villaseñor, 1995). In particular, the SFZ (Fig. 1) is the principal structure of the Hispaniola restraining bend and was the locus of very large earthquakes in the past (Russo and Villaseñor, 1995). The seismic region is associated with the EFZ (Fig. 1) located in Hispaniola's southern peninsula in its southern part (SZ32–SZ34). A zone of northwest–southeast–trending thrust faults lies between the eastern end of the EFZ and the western portion of the SFZ (Mann *et al.*, 1995; Lundgren and Russo, 1996).

Seismic Region Jamaica (SZ35, SZ36). It is associated with the left-lateral strike-slip Walton fault in its northern part, which extends from the southeastern margin of the CSC to PGFZ. The strong earthquakes of Jamaica in 1692 (M 7.75) and 1907 (M 6.6) were located on the northern side of the island, on the southern slope of the Bartlett Trough. The southern part of this seismic region constitutes the northern margin of the Caribbean plate (Mann *et al.*, 1995). Onshore in southeastern Jamaica, the east–west–striking Plantain Garden fault has a slip rate of 5–7 mm/yr along its length.

Seismicity Rates

The seismicity rate of each magnitude or intensity class (both are 0.5 units) within each SZ is given as the number of earthquakes counted in a time interval for which the catalog is complete for that magnitude or intensity. Using discrete seismicity rates, instead of interpolating the data with the Gutenberg–Richter relation, leads to two main advantages (see more discussion in Rebez and Slejko, 2000):

1. If different return periods are considered, the hazard assessment changes significantly as a function of the different seismic energy release in time, while, using the Gutenberg–Richter relation, different return periods produce only a homogeneous raising (or lowering) of hazard;
2. It is possible to adequately describe those SZs with a characteristic earthquake behavior.

The catalog completeness was evaluated for three subcatalogs: east-central Cuba; western Cuba; and Jamaica, Hispaniola, and Puerto Rico. For each subcatalog, the completeness periods were identified roughly by a historical analysis, that is, identifying periods when the data collection of natural phenomena was homogeneous (because of the presence of convent archives, installation of seismographic stations, etc.). In this framework, a statistical analysis was performed by investigating the total number of events in time (Stepp [1972] plots) to precisely identify the completeness period for each magnitude class. The completeness periods calculated are similar for the three subcatalogs, with the exception of east-central Cuba, where large ($M > 6.0$) earthquakes are missing (Table 3; Fig. 7).

For each magnitude or intensity class, the completeness period was used to compute the seismicity rates by counting the earthquake number in each class during those time periods and then normalizing the number to 100 years. The procedure for adequately determining the seismicity rates was established on an objective basis (see Slejko *et al.* [1998] for more details). In fact, the completeness period of each class identifies the preliminary seismicity rate and, consequently, its related return period ($T = 100$ years/seismicity rate). If a higher seismicity rate that is related to a time period not shorter than the return period of the preliminary seismicity rate exists, this higher value is chosen. If a higher seismicity rate that is related to a period shorter than the completeness period but longer than the return period of the class exists, this higher value is taken.

Table 3
Completeness

M	All catalog	Zone A	Zone B	Zone C
2.0	1980	1980	1970	1980
2.5	1970	1980	1970	1980
3.0	1970	1940	1940	1970
3.5	1960	1940	1940	1970
4.0	1940	1940	1900	1940
4.5	1900	1900	1900	1900
5.0	1850	1900	1850	1800
5.5	1800	1850	1700	1800
6.0	1760	1800	1700	1700
6.5	1700		1500	1600
7.0	1500		1500	1500
7.5	1500		1500	1500
8.0	1500		1500	

Zone A, east-central Cuba; Zone B, western Cuba; Zone C, Jamaica, Hispaniola, and Puerto Rico.

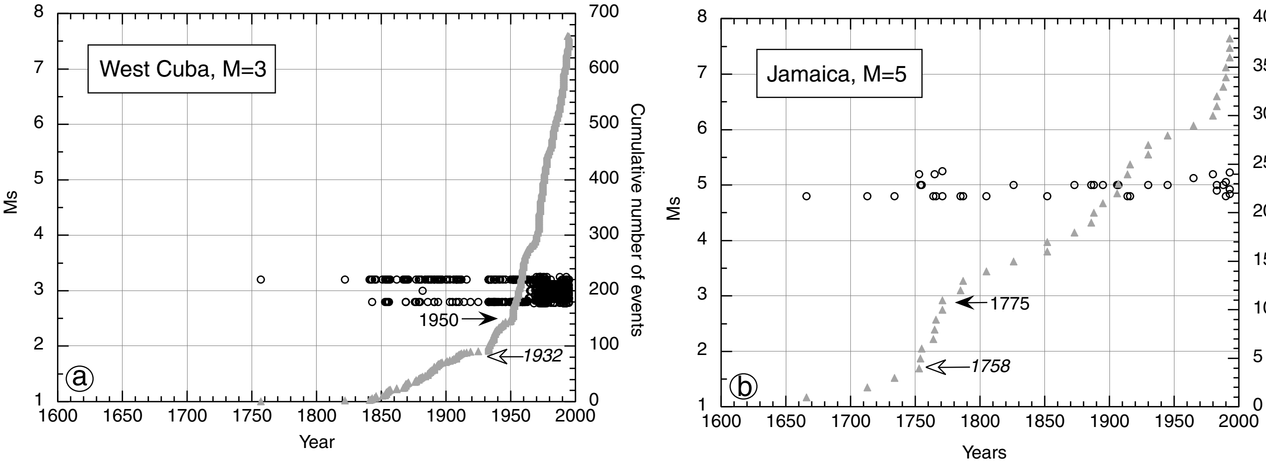

Figure 7. Examples of two Stepp (1972) plots: (a) M class 3 ($2.8 \leq M \leq 3.2$) for western Cuba; (b) M class 5 ($4.8 \leq M \leq 5.2$) for Jamaica, Hispaniola, and Puerto Rico. The open dots represent the earthquake magnitude and the triangles the annual cumulative number of events. The white arrows show the beginning of the complete period according to the historical information, and the black arrows indicate the complete period chosen in this study.

Magnitude Seismicity Rates

Figure 8a shows the contributions of small- ($M < 3.8$), moderate- ($3.8 \leq M \leq 5.8$), and large-magnitude ($M > 5.8$) earthquakes to the seismicity rates (number of events normalized to 100 years) for each SZ. The values were obtained by simple summation of the individual rates. This picture clearly shows two different behaviors, the first regarding the intraplate seismicity (from SZ1 to SZ25), the second related to the more active interplate seismicity (from SZ26 to SZ36). The behavior of the intraplate SZs is characterized by a general, similar pattern in the magnitude ranges: SZ8 has an abundance of small-, moderate-, and large-magnitude earthquakes, whereas SZ2 does not; SZ5 abounds in large- and small-magnitude earthquakes but misses moderate-magnitude ones, perhaps because of an incorrect magnitude evaluation. A unusual behavior can be seen in some neighboring SZs, such as SZ16 and SZ17, where the first abounds in moderate-magnitude earthquakes but the second has small ones. Again, an incorrect magnitude estimation or an epicenter mislocation can be invoked. A better agreement among the number of events in the three magnitude ranges can be seen in the interplate SZs, where SZ31 is the most active. Inconsistencies in the relative numbers of large and small earthquakes can be explained by incomplete event detection and the shortness of the historical record.

An important parameter for the SZ seismicity definition is the maximum magnitude value (M_{max}). The geological complexity of the Caribbean region and the incomplete knowledge of seismotectonic processes sometimes prevent a clear assignment of seismicity to specific tectonic structures. For this reason, it was decided to introduce an M_{max} following two procedures. Where the number of earthquakes is large, the rates were fitted by the Gutenberg–Richter relationship, and the extrapolated rate for a magnitude greater than the maximum observed value by one step unit (0.5 in our case: one-step-beyond technique [Slejko *et al.*, 1998]) was considered if it involved a mean return period of between 500 and 1500 years, that is, larger than the time window of the catalog. This 500- to 1500-year return period, in fact, might involve events missing in the catalog, but it is not too long to account for events with a very low rate. In such a way it was possible to assign the M_{max} to 15 SZs, marked by asterisks in Table 4. For the other SZs, where it was not possible to obtain an M_{max} on a seismological basis, the value suggested by various authors (Cotilla *et al.*, 1991; Gonzalez *et al.*, 1993; Chuy and Alvarez, 1995; Rodriguez *et al.*, 1997) from tectonic/geologic evidence was considered and a value in between was taken. In such a way, the M_{max} was assigned to 15 SZs, marked by double daggers in Table 4. For a few SZs with a low maximum observed magnitude, the seismotectonic/geologic-based M_{max} seems to overestimate the actual capability of the seismogenic structures involved. This is due to the fact that the geological M_{max} was estimated by Cuban geologists on the basis of the total fault lengths without considering their segmentations. An M_{max} lower than the minimum seismotectonic/geologic-based M_{max} was taken in these cases for six SZs marked with daggers in Table 4.

Intensity Seismicity Rates

The same procedure used for defining the SZ seismicity rates in terms of magnitude was followed for defining the seismicity rates in macroseismic intensity. All our catalog's entries coming from the Chuy (1999) catalog have an intensity value; for the remaining events without intensity, this parameter was calculated from magnitude using the empirical relation by Fedotov and Shumilina (1971).

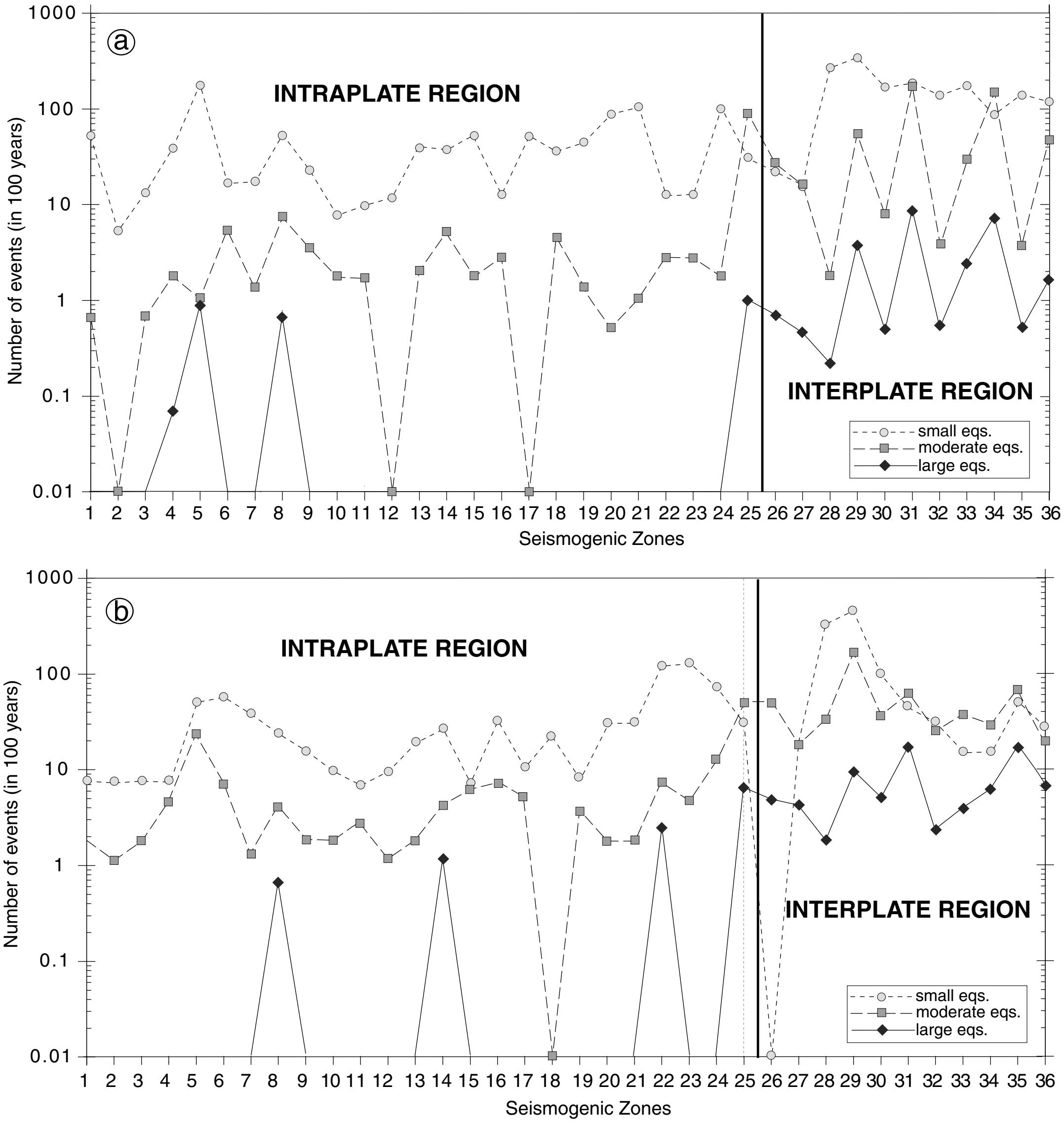

Figure 8. SZ seismicity rates (number of earthquakes in a 100 years) for small earthquakes (short-dashed line: $M < 3.8$, $I_o \leq$ IV–V), moderate earthquakes (dashed line: $3.8 \leq M \leq 5.7$, V $\leq I_o \leq$ VI–VII), and large earthquakes (solid line: $M > 5.7$, $I_o \geq$ VII): (a) for magnitude classes; (b) for intensity classes.

No maximum intensity values were added to the intensity rates, because it is impossible to predict that an hypothetical, future, larger earthquake will produce more severe damage than the damage already undergone, considering the improvement of building design with time. Moreover, caution has driven the choice of the intensity attenuation relation, as described in the following section.

The intensity rates (Fig. 8b) show remarkable differences with respect to those for magnitude (Fig. 8a), although the higher seismicity of the interplate SZs clearly appears again. These differences can be explained by the possible poorer correlation between magnitude and intensity for offshore earthquakes. Nonetheless, SZ8 is again one of the most active among the intraplate SZs and SZ31 among the interplate ones.

Attenuation Relationships

Macroseismic intensity (I_s), in the MSK scale, was the commonly used parameter for seismic hazard assessment and seismic building code definition in Cuba (Chuy *et al.*, 1983). Those results were converted into PGA values (in centimeters per second squared) through the use of the Trifunac and Brady (1975) empirical relationship:

$$\log(\mathrm{PGA}) = 0.30\, I_s + 0.014. \qquad (10)$$

The disadvantage of transforming intensity into PGA by a general relationship is that linear relationships linking PGA to I_s are characterized by large uncertainties (Reiter, 1990). More detailed studies (Murphy and O'Brien, 1977) on PGA–

Table 4
M_{max} Values for the SZs

SZ	M_{obs}	M_A	M_B	M_C	M_D	ΔM	M_{max}
1*	4.5	7.0	5.3	5.5	7.0	5.3–7.0	5.0
2†	4.0	7.0	6.0	7.0	7.0	6.0–7.0	5.0
3‡	4.0	7.0	5.6	5.2	7.0	5.2–7.0	5.2
4‡	5.5	7.0	6.5	7.0	7.0	6.5–7.0	6.5
5*	6.0	6.5		6.5	7.0	6.5–7.0	6.5
6‡	5.0	7.0		7.0	6.5	6.5–7.0	6.5
7†	4.0	6.0		5.5	6.0	5.5–6.0	5.0
8‡	6.0	7.0		6.3	7.0	6.3–7.0	7.0
9‡	4.0	6.0		5.0	6.5	5.0–6.5	5.0
10‡	4.0	6.0		5.2	6.0	5.2–6.0	5.5
11*	5.0	6.5	5.5	5.5	6.5	5.5–6.5	5.5
12†	3.5	6.0	5.5	5.5	6.0	5.5–6.0	5.0
13‡	4.0	6.5	5.5	5.8	6.5	5.5–6.5	5.5
14†	4.5	7.0	5.8	5.8	7.0	5.8–7.0	5.5
15‡	4.5	6.5	6.0	6.0	6.5	6.0–6.5	6.0
16‡	5.0	6.5	5.5	5.5	6.5	5.5–6.5	6.0
17‡	3.0	6.5	5.0	5.0	6.0	5.0–6.5	5.0
18‡	4.5	6.5		5.5	6.0	5.5–6.5	6.0
19‡	6.0	6.5		7.0	7.0	6.5–7.0	7.0
20*	6.5	7.0	7.0	7.0	7.0	7.0	7.0
21†	4.5	6.5		6.5	6.5	6.5	6.0
22‡	4.5	6.5	6.0	6.5	5.0	5.0–6.5	6.0
23‡	4.5	6.5		6.5	6.0	6.0–6.5	6.0
24†	4.0	6.5		6.5	6.0	6.0–6.5	5.5
25*	6.5				8.0	8.0	7.0
26*	6.5				8.0	8.0	7.0
27*	7.2				8.0	8.0	7.5
28‡	7.0	8.0		8.0	7.5	7.5–8.0	8.0
29*	7.5	8.0		8.0	8.0	8.0	8.0
30*	7.5	8.0		7.6	7.5	7.5–8.0	8.0
31*	8.2			8.3	8.3	8.3	8.5
32*	7.0			6.0	7.6	6.0–7.6	7.5
33*	7.7			8.0	7.6	7.6–8.0	8.0
34*	7.5			7.6	7.6	7.6	8.0
35*	7.0			7.0	7.0	7.0	7.5
36*	7.5			7.6	7.6	7.6	8.0

*M_{max} chosen on seismological basis.
†M_{max} chosen on specific considerations (see text).
‡M_{max} chosen on tectonic/geologic basis.
The SZ code refers to Figure 6; the other columns are M_{obs}, maximum observed magnitude in the catalog; from M_A to M_D, maximum magnitude on tectonic/geologic basis from the literature (A, Cotilla *et al.*, 1991; B, Gonzalez *et al.*, 1993; C, Chuy and Alvarez, 1995; D, Rodriguez *et al.*, 1997); ΔM, range of the tectonic/geologic M_{max} estimates; M_{max}, maximum magnitude used in this work.

intensity relationships led to multivariate relationships, PGA $= f(I_s, D, M)$, as magnitude, epicentral distance, and site conditions strongly influence the level of peak ground motion predicted for a given intensity.

Although PGA does not represent the complete ground shaking, being a single point that does not consider important factors such as the number of cycles, duration, frequency, and energy content, it is still used worldwide for establishing design criteria. Macroseismic intensity also remains a useful parameter for loss estimates. In the present work, we decided to follow the standard probabilistic approach, which consists of using PGA attenuation relations, in spite of the fact that none of them has been tested for the Caribbean region. In addition, seismic hazard estimates in terms of macroseismic intensity were computed for two main reasons. The first is the need to compare the PGA estimates with those based on intensity, where specific intensity attenuation relations have been calibrated on Cuban data. A second reason was the need to also consider local attenuation relations among those used for the final hazard map. To accomplish this, the hazard results in terms of intensity have been simply translated into PGA values by the Trifunac and Brady (1975) relation, as in previous Cuban works. The map thus obtained can be compared directly to that for PGA, the differences being due to the individual intensity attenuation relations used, which were calibrated on macroseismic data actually observed on Cuban territory. For these reasons, great emphasis is given to the problem of PGA and intensity attenuation in the present work.

PGA Attenuation Relations

Strong motion relationships to be used in seismic hazard assessment form an essential input and have a strong influence on the results. General relations valid over very large regions can be found in the literature when local relations are not available. Such attenuation relationships for Cuba, as well as for the eastern Caribbean, do not exist. For this reason we decided to consider three PGA attenuation relationships for average soil: Joyner and Boore (1981), Quijada *et al.* (1993), and Ambraseys (1995). Average soil conditions are motivated by the unavailability of soil-type maps of the study area, and the choice of the relations is also based on their direct applicability to SEISRISK III (Bender and Perkins, 1987), the computer code we use for seismic hazard assessment.

The Joyner and Boore (1981) and Ambraseys (1995) relationships are commonly used in North America and Europe, respectively. The Quijada *et al.* (1993) relation (see Dimaté *et al.*, 1999) refers to Venezuela, where tectonic regimes similar to those in the Caribbean can be found. All the relations are azimuth independent and do not consider the intrinsic differences of the SZ tectonic regime (compressional, tensile, transcurrent, volcanic, etc.).

Joyner and Boore (1981) derived an equation using recordings generated by earthquakes in western North America. It is defined for moment magnitude, in the range $5.0 \leq M_w \leq 7.7$:

$$\log \mathrm{PGA} = -1.02 + 0.249M_w - \log (R^2 + 7.32)^{1/2} - 0.000255\,(R^2 + 7.32)^{1/2}, \quad (11)$$

where PGA is in gravitational acceleration (g) and R is the shortest distance to the surface projection of the fault rupture in kilometers. The relation is calibrated in the distance range 0.5–350 km, but it is applied at distances less than 200 km (http://geohazards.cr.usgs.gov/eq) and has a standard deviation (σ) of 0.26. The M_s values in our catalog were transformed into M_w values using the relations obtained by Tanner and Shepherd (1997) for the Caribbean region (see Shedlock, 1999).

Quijada *et al.* (1993) used the following relation for crustal sources in the seismic hazard assessment of the northern Andes (Dimaté *et al.*, 1999) under the GSHAP project:

$$\ln \mathrm{PGA} = 5.40 + 0.36M_s - 0.86 \ln (R + 10), \quad (12)$$

where PGA is in centimeters per second squared and R is the epicentral distance in kilometers. The relationship has a σ of 0.66.

Ambraseys (1995) used an extensive data set (1260 records for 619 European earthquakes) obtained in the free field or from the base of buildings with no more than three stories. The relation was calibrated in the range $2.0 \leq M_s \leq 7.3$ and in the distance range 1–310 km:

$$\log \mathrm{PGA} = -1.43 + 0.245M_s - 0.786 \log (R^2 + 2.72)^{1/2} - 0.001\,(R^2 + 2.72)^{1/2}, \quad (13)$$

where PGA is in gravitational acceleration and R is the distance from the fault in kilometers, which for small earthquakes corresponds to epicentral distance. The σ is 0.24.

In Figure 9 the behavior of the previous attenuation relations (with and without σ) for two classes of magnitude ($M_s = 5.0$ and $M_s = 7.0$) is shown. As our seismic sources are wide zones rather than individual faults, the three different distances are identified as similar. The highest PGA values in both cases are given by the Joyner and Boore (1981) relation in the near field, while for distances greater than 100 km the Quijada *et al.* (1993) relation gives higher values. All three relations, equally weighted, were used in a logic-tree approach (McGuire, 1977; McGuire and Shedlock, 1981; Kulkarni *et al.*, 1984; Coppersmith and Youngs, 1986).

Intensity Attenuation Relations

For this study attenuation relationships have been developed for macroseismic intensity. The attenuation curves were derived from the most important earthquakes, following formulations of intensity decay proposed by different authors (von Kovesligethy, 1907; Blake, 1941; Grandori *et al.*, 1987; Berardi *et al.*, 1994).

The macroseismic intensity relationships proposed here are strictly for the purpose of seismic hazard evaluation and are not intended to describe either the physical properties of the crust or the seismogenic processes involved. The final attenuation relationships will be linked to the proposed seismogenic zonation (Fig. 6).

Database

The database of macroseismic observations was collected by Chuy (1999) and partially revised and georeferenced during this work. Intensity data points have been compiled using information contained in chronicles, the press, and technical reports of damage, according to the MSK scale. The macroseismic catalog proposed by Chuy (1999) contains 1513 perceptible events for the Cuban region from 1528 (the first historical earthquake reported in the Spanish chronicles) to October 1996.

Keeping in mind the number of intensity points reported for each earthquake and the existence or nonexistence of an isoseismal map, we made a preliminary selection of 121 events for which the macroseismic parameters (epicentral coordinates, magnitude, $I_0 = I_{\max}$, and depth) exist. Due to the small number of observed intensities, it was necessary to reduce the population to 69 events (Table 5), so that each

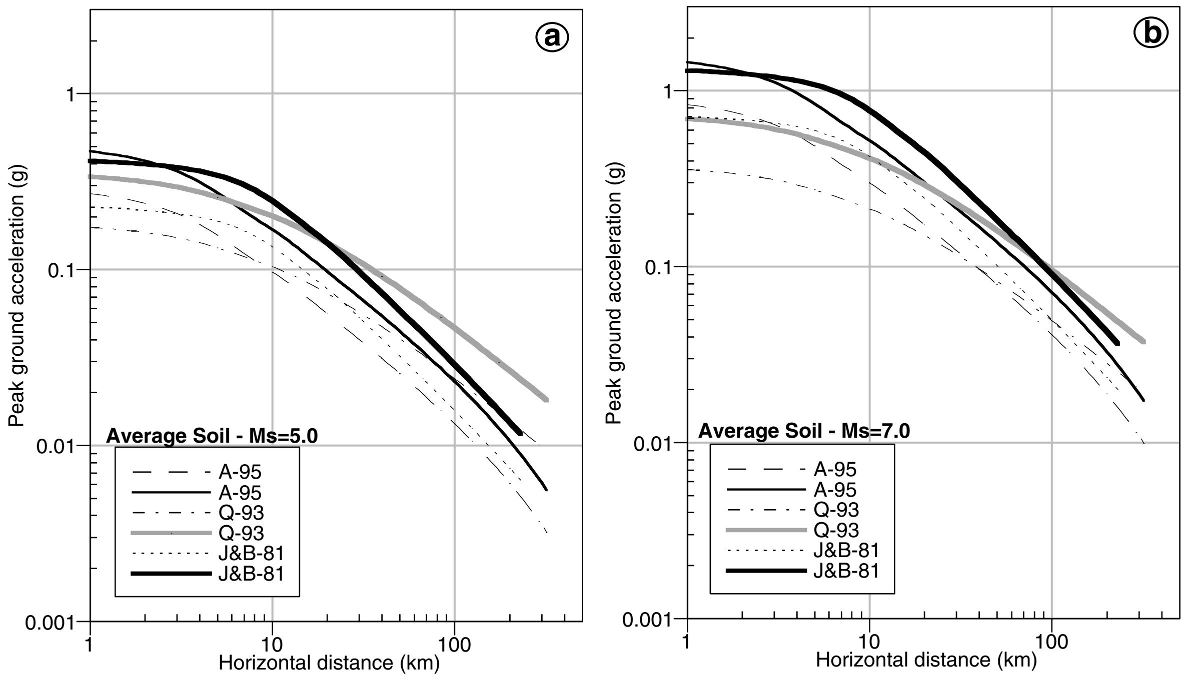

Figure 9. Comparison among the PGA attenuation relations considered in the present study (A-95, Ambraseys; 1995; Q-93, Quijada *et al.*, 1993; J&B-81, Joyner and Boore, 1981) with (solid lines) and without (dashed lines) σ: (a) for M_s 5.0; (b) for M_s 7.0.

earthquake has at least three intensity classes, each with at least three data points.

We next analyzed the macroseismic data set, which consists of a list of localities with given coordinates and intensity related to an earthquake. The macroseismic epicenter and epicentral intensity correspond to the values reported in the earthquake catalog (Chuy, 1999). Ranges in intensity assessment (i.e., uncertain determination), usually given by the minimum and maximum intensity values (e.g., V–VI; see Table 5), are treated by assigning one sample to both the intensity classes with an associated weighting factor that will be described later.

Table 5 contains the main information regarding the 69 selected events. The SZ codes refer to Figure 6; the date, epicentral coordinates, and maximum intensity were taken from previous works (Chuy, 1999). The N value is the number of intensity points per event, and N^* is the number of samples in each intensity class. Not all these data may be analyzed (Fig. 10), as a significant amount of intensity points do not have the locality coordinates or refer to sites where the earthquake was not felt ($I_S <$ II MSK). On average each SZ has about 100 usable intensity points, with a minimum of less than 10 points in SZ9 and a maximum of more than 700 observations in SZ29.

From Data Points to Attenuation

After an analysis of different attenuation models, we decided to follow the Italian experience (Peruzza, 1995, 1996, 2000) of calibrating attenuation relationships for each SZ to a single well-documented earthquake. We adopted, therefore, some different well-known formulations and a semiautomatic procedure in order to derive the unknown coefficients of each relationship.

The selected models are as follows:

1. The von Kovesligethy (1907) relationship:

$$I_0 - I_i = 3\log\frac{\sqrt{D_i^2 + h^2}}{h} + m\left(\sqrt{D_i^2 + h^2} - h\right), \quad (14)$$

   where I_0 indicates the epicentral intensity, I_i the intensity at the ith site, and D_i its epicentral distance; h and m are parameters to be estimated from experimental data.
2. The Blake (1941) model:

$$I_0 - I_i = a\log\sqrt{\frac{D_i^2 + h^2}{h}}, \quad (15)$$

   where a and h are the unknown coefficients; usually h is intended as the hypocentral depth.
3. The relationship proposed by Grandori *et al.* (1987):

$$I_0 - I_i = \frac{1}{\ln\psi}\ln\left[1 + \frac{\psi - 1}{\psi_0}\left(\frac{D_i}{D_0} - 1\right)\right], \quad (16)$$

   where ψ, ψ_0 and D_0 are unknown coefficients.
4. The formula proposed by Berardi *et al.* (1994):

Table 5
Earthquakes Suitable for the Calibration of the Attenuation Relationships

SZ	Date			Imax	Coordinates		N	N*													
	Year	Month	Day		Lat	Long		Not felt	II	II-III	III	III-IV	IV	IV-V	V	V-VI	VI	VI-VII	VII	VII-VIII	VIII
4	1992	09	25	IV	22.65	79.40	25	6	10		6		3								
5	1914	08	25	VII	21.22	76.17	47	4			1		4	2	12	4	10	5	5		
5	1953	09	20	V-VI	22.10	78.60	17	1					5	4	6	1					
8	1880	01	23	VIII	22.70	83.00	89	7				2	2		10	6	15	9	21	6	11
9	1957	09	11	V	22.18	83.65	17	6			3	3	2	2	1						
11	1982	12	16	VI	22.60	81.40	134				20	13	28	17	32	14	8				
13	1984	05	16	IV-V	22.93	80.50	34	11		1	12	2	6	2							
14	1939	08	15	VII	22.65	79.40	43	1			1	1	6	1	11	9	8	3	2		
14	1960	05	25	V	22.45	79.48	11				3	1	6		1						
15	1953	01	01	VI	22.10	78.60	55	1			4	11	13	12	9	4	1				
16	1972	06	27	V	21.81	78.09	13				3	1	5	1	3						
16	1974	04	08	VI	21.86	78.05	63				27		23		9		4				
16	1974	11	05	V	21.97	78.20	14	10			2				2						
16	1995	04	05	IV	22.05	77.80	36			4	6		2		24						
17	1987	07	07	IV-V	19.92	75.62	54	3		2	17	15	14	3							
18	1980	03	11	IV-V	21.13	76.58	7				2	2	2	1							
18	1954	12	16	V	20.86	76.36	13	2		1			4	2	4						
19	1962	07	19	VI	20.52	77.20	16	3				2	6		2	2	1				
19	1987	04	11	IV	20.43	76.69	55	8			26	14	7								
19	1987	04	25	IV-V	20.41	76.65	61	12		2	18	17	11	1							
19	1988	03	27	IV	20.43	76.73	30	6		3	6	6	9								
19	1988	03	29	IV	20.42	76.72	31	10	1	2	8	9	1								
20	1984	02	23	IV	19.91	75.41	17				7	4	6								
20	1985	09	01	V	19.70	75.35	58	4			7	3	16	8	20						
20	1989	03	27	IV	19.93	75.40	37	8	4	7	6	6	6								
20	1989	06	21	IV	19.82	75.40	50	8	5	5	14	12	6								
20	1992	10	02	III-IV	19.77	75.45	12	5		2	2	3									
20	1993	04	05	IV	19.94	75.36	15	4		2	2	4	3								
22	1943	07	30	VI	21.85	80.10	41	10			2	3	9	2	9	3	3				
22	1996	08	08	IV-V	21.75	80.30	25	7		4	5	3	5	1							
28	1989	02	15	III-IV	19.66	78.12	20	6	2	5	2	5									
28	1992	05	25	VII	19.44	77.83	111		1	3	8	4	16	9	21	5	35		9		
28	1992	05	26	V	19.64		16	4		5	2	1	3		1						
28	1992	05	27	IV	19.66	77.68	6		2	4	5	3	3								
28	1992	05	28	III-IV	19.66	77.70	8	3	2	1		2									
29	1932	02	03	VIII	19.75	75.58	64				1		4	2	9	11	11	5	13	3	5
29	1968	10	11	VI	19.88	75.92	36		1		4	3	8	2	17		1				
29	1978	11	13	VI	19.85	76.02	18				4		5	3	5		1				
29	1983	12	01	V	19.93	75.96	42				4	8	11	8	11						
29	1984	05	05	IV	19.85	75.84	32	7			8	11	6								
29	1984	08	20	III-IV	19.92	76.47	29	13	13	6	6	2									
29	1984	10	21	IV	19.93	75.79	16	3			5	3	5								
29	1985	11	14	III-IV	19.87	75.93	12	5			1	6									
29	1986	01	07	IV	19.80	75.68	12	2			1	3	6								
29	1986	10	03	IV	19.80	75.40	16	6		1	5	1	3								
29	1987	07	08	IV	19.89	75.62	20	5			6	3	6								
29	1988	01	05	IV-V	19.87	75.43	69	7			12	19	26	5							
29	1988	03	20	IV	19.86	75.52	47	5			18	11	13								
29	1988	07	04	IV-V	19.83	75.65	23	7		6	2	4	3	1							
29	1988	11	12	IV	19.16	76.74	76	12		11	27	17	9								
29	1989	03	01	III	19.85	75.61	21	8	4	3	6										
29	1989	03	06	III-IV	19.77	76.20	22	7		5	8	2									
29	1989	04	14	IV-V	19.86	76.90	35	4	1	10	6	4	8	2							
29	1989	07	10	IV	19.87	75.94	44	7	5	4	12	9	7								
29	1989	07	19	IV	19.93	76.05	20	4		3	4	5									
29	1989	08	06	IV-V	19.84	75.74	33	7	1	4	7	4	8	2							
29	1989	10	31	IV-V	19.84	75.45	23		1	4	3	7	6	2							
29	1990	01	06	IV-V	19.74	77.12	32	5	2	4	8	4	6	3							
29	1992	07	24	IV	19.84	76.54	21	3	1	2	6	7	2								
29	1992	11	06	IV-V	19.76	76.30	19	4			3	6	2	4							
29	1992	11	07	IV-V	19.66	76.34	22	3		1	4	8	5	1							
29	1992	12	18	IV	19.89	76.44	12	4			3	2	3								
29	1993	05	24	IV-V	19.82	75.74	26	3	1	3	3	6	5	5							
29	1993	11	28	IV	19.90	76.21	27	5	9	3	5	2	3								
30	1947	08	07	VII	19.75	75.70	33	1				1	3	2	11	2	6	4	3		
30	1984	04	21	IV	19.85	74.29	25	7				4	11	3							
30	1984	05	03	V	19.85	75.30	50	8			6	13	17	3	3						
30	1987	11	15	IV	19.90	75.32	20	4		3	6	5	2								
30	1988	12	10	IV	19.86	75.20	56	3		4	21	23	5								

The SZ code refers to Figure 6; fields from Date to N derive from the catalog. N indicates the total number of intensity points available, while N* represents the number of points in each intensity class.

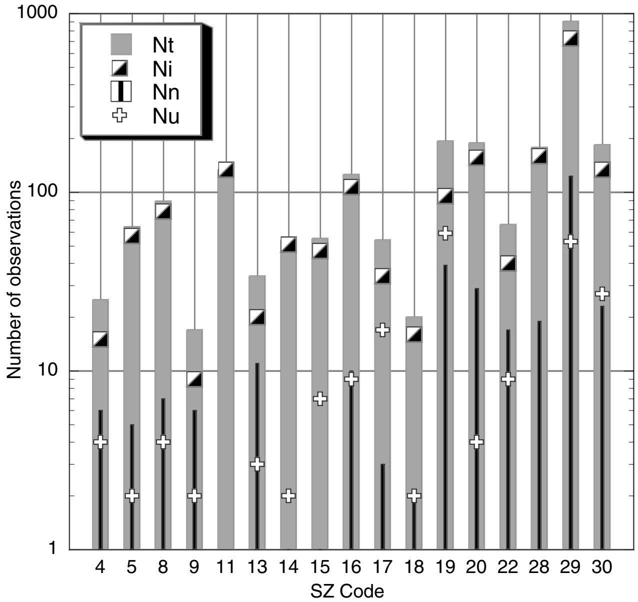

Figure 10. Number of intensity data points in the SZs. N_t represents the total number (for all earthquakes in the SZ) of points with intensity ≥II MSK, N_u indicates the number of points with unknown coordinates, N_n shows the number of points where the earthquakes were not felt, and N_i is the number of usable points: $N_t = N_i + N_n + N_u$.

$$I_0 - I_i = \alpha + \beta^3 \sqrt{D_i}\,, \qquad (17)$$

where α and β are unknown coefficients, and I_0, I_i, and D_i have the same meaning as before.

The procedure applied here computes the unknown coefficients directly from the actual intensity points of the selected earthquake without using isoseismal maps. Four main steps follow:

1. Computation of epicentral distance for each locality where the observed intensity value is available.
2. Construction of the sample cumulative curve of distances corresponding to the same macroseismic value; intensity ranges (i.e., uncertain estimates, such as VI–VII for example) are split into two classes using the weighting factor

$$w_{obs} = 1/[(I_{max} - I_{min}) + 1]. \qquad (18)$$

Figure 11 illustrates these curves for two well-documented earthquakes.
3. Computation of the distance not expected to be exceeded at a 50% probability for each intensity class, associated with its intensity decay ($I_0 - I_i$). This application utilizes the median value (50% empirical sample percentile) compatible with the rounding that transforms real values of intensity into integers.
4. Application of a nonlinear least-squares regression to the distance–intensity decay pairs, to derive the unknown coefficients of equation (14) to equation (17).

The proposed method has the advantage of being completely transparent and reproducible, establishing some rules for attenuation-curve fitting using macroseismic data that can be applied to any attenuation model.

Two of the models (equations 16 and 17) were selected following the Italian experience: in particular in the Grandori *et al.* (1987) formula the presence of the D_0 parameter determines intensity values greater than I_0 (i.e., negative intensity decay) near the source, an important peculiarity in the group of intensity attenuation relations. Common practice truncates the curve with a flat step of zero decay, for distances smaller than D_0 introducing a circular model of extended source that gives a better approximation than the point source model. The formulation with three coefficients makes the relation very flexible, even if quite unstable; the curve may simulate a logarithmic-shaped curve, linear decay of intensity with distance, and also an unusual increase of the decay rate. The two other models (equations 14 and 15) are frequently used; the von Koveslighety (1907) formula in particular has been widely adopted in many Cuban studies (Alvarez and Bune, 1977; Chuy and Alvarez, 1995; Rodriguez *et al.*, 1997).

Data Analysis

Figure 12a shows some examples of curve fitting for earthquakes in SZ29; the different attenuation relations are compared for two earthquakes. Note that the curves are very similar at distances greater than 30–40 km, as in the case of the 1932 earthquake, which is the best documented one. The major differences between models are in the near fields, as the Berardi *et al.* (1994) and Grandori *et al.* (1987) formulations permit negative values of intensity decay. The agreement among the fits, with the different attenuation models, testifies to the good quality of the data as well as to the robustness of the fitting. Figure 12b shows the behavior of six earthquakes in SZ29 (Table 5), all modeled by the Berardi *et al.* (1994) formulation. The attenuation of the 1932 earthquake is the slowest and, consequently, represents the most conservative choice for the attenuation of SZ29. These two aspects were considered as guidelines in the choice of the representative earthquake for each SZ.

From the 69 initially selected earthquakes, only the representative one for each SZ was kept. As the data available for SZ4, SZ9, SZ13, SZ17, and SZ18 did not give an acceptable fit, we finally selected only 12 good intensity maps that represent the attenuation in 12 SZs (Table 6).

The coefficients obtained according to the four models are reported in Table 7: the formulation selected is the one that best fits the data and appears in bold. The statistical errors of the unknown coefficients are not reported in the table, as they are not representative of the actual error in the attenuation relationship (see more discussion later).

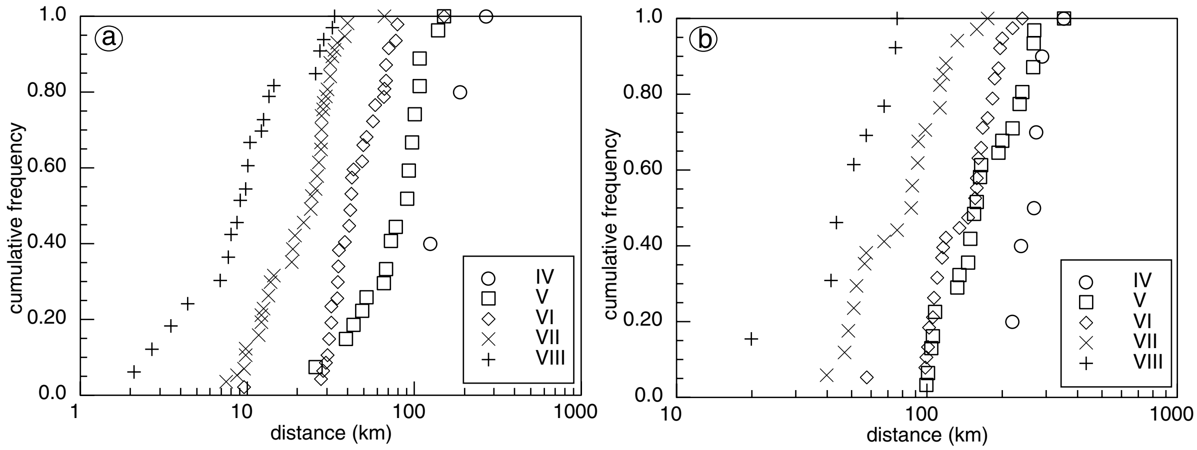

Figure 11. Sample cumulative curve of epicentral distances for two main Cuban earthquakes: (a) event of 23 January 1880 in SZ8; (b) event of 3 February 1932 in SZ29.

An average attenuation relation for the whole study region was also obtained, considering only the simpler formulations (equations 15 and 17) and using all the observations with intensity larger than, or equal to, III MSK. The best fit was reached for the Berardi *et al.* (1994) formulation, whose coefficients are shown in Table 7; the related curve is reported in Figure 12b for comparison.

The one-source/one-attenuation relationship was the ultimate solution; the average relation was used only when data for establishing a specific relationship were not sufficient. The choice of one relation for each SZ was motivated by several facts. One is that inside many SZs, the ground motion exhibits different attenuation properties. Another is based on the fact that we are not able to ascertain the source, path, and site effects. Furthermore, we are not able to evaluate either the bias, due to insufficient spatial sampling, or the influence related to different data set compilers. The earthquake used to model the attenuation is usually the strongest event that occurred in the SZ. In other cases, we have only one well-documented earthquake in the SZ; in this situation, our only choice is to use it. In such a way, the final attenuation coefficients were associated with the seismogenic zonation proposed in Figure 6, where gray areas indicate the 12 SZs that have their own intensity attenuation relationship.

Reliability

The reliability of the attenuation relationships previously obtained cannot be simply expressed in terms of statistical errors of the fitted curve, because the use of the 50% fractile distance artificially reduces the variance of observed data. This is the reason that the statistical errors obtained in the minimization procedure for the unknown coefficients are not reported.

Therefore, the quality of the attenuation curves has been evaluated in terms of residuals with respect to the observations. The mean residual (MR) is defined as

$$\mathrm{MR} = \sum_{i=1}^{N} |I_{\mathrm{obs}_i} - I_{\mathrm{cal}_i}| \Big/ \sum_{i=1}^{N} w_i \,, \tag{19}$$

where w_i indicates the weight given to each observation and N is the total number of intensity points. As the modulus of the residual is considered, the MR represents the most conservative error evaluation. The MR can be computed for the data for one earthquake or for data for each intensity class.

Figure 13 plots the MRs obtained for the 12 representative earthquakes, for each intensity class; small dots indicate the MR values obtained using the best-fitting attenuation relationships (type and coefficients enhanced in bold in Table 7), while the open squares are the MR values obtained considering the average attenuation relationship.

The MRs of the SZ-specific attenuation relationships oscillate around the value of 1.0, a value that is comparable with the reliability of the intensity data. Three cases exhibit an MR greater than 2, and they always refer to very few data points, where the 50% fractile distance loses its meaning and the local high residuals (for example due to site response) cannot be smoothed by other observations (small Σw_i in equation 19).

On the other hand, the MR values obtained considering the average attenuation relationship (whose parameters have been obtained by fitting all intensity decay–distance pairs) are higher and increase on average from 2.5 to 3.5 with intensity class. The poorer reproduction of the highest shaking, using an average attenuation relationship, has also been recognized in the Italian data set (see Peruzza, 2000).

We may argue that using multiple attenuation coefficients significantly improves the macroseismic predicted values, unlike when employing a single average relationship. In fact, the use of different coefficients in the Grandori *et al.* (1987) formulation, which provides a zero decay for distances smaller than D_0, better simulates the near-field behavior, while the Berardi *et al.* (1994) average relationship

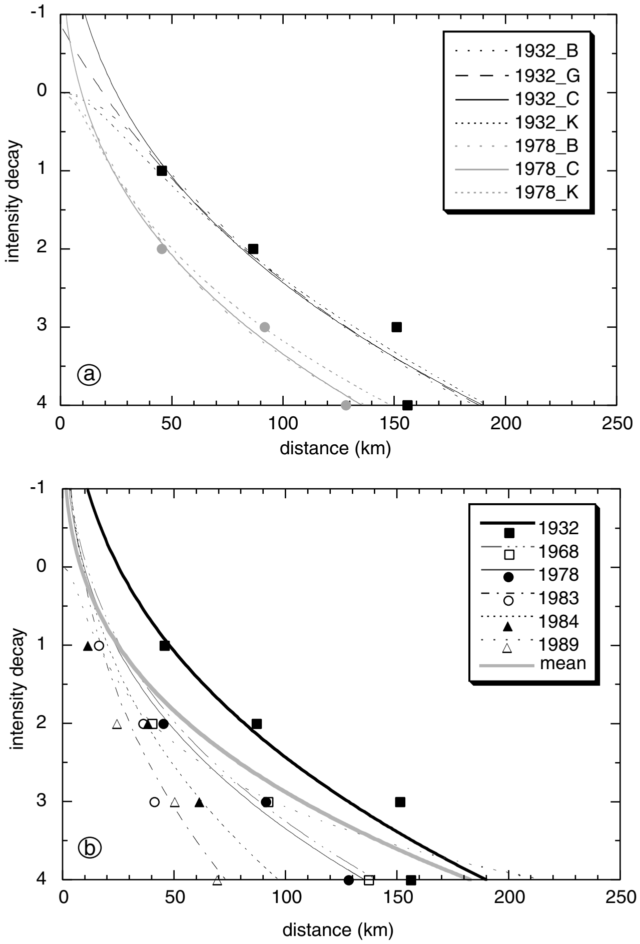

Figure 12. Curve fitting for earthquakes in SZ29: (a) the von Kovesligethy (1907) (K), the Blake (1941) (B), the Grandori *et al.* (1985) (G), and the Berardi *et al.* (1994) (C) attenuation relations are applied to the 1932 and 1978 earthquakes; the filled squares and circles show the data points. (b) The intensity points of six earthquakes are fitted by the Berardi *et al.* (1994) attenuation relation. The gray solid line represents the average general relation obtained for the whole study region.

systematically underestimates the intensities near the epicenter.

A complete statistical analysis of the residuals, earthquake by earthquake, is not presented here. It will be investigated in a separate article, since a proper approach to attenuation reliability should consider both local soil conditions and a quality factor of each macroseismic data point.

The standard deviations of each intensity class for each representative earthquake have no practical use; a σ of about 0.9 intensity units may be considered a reasonable average of all the MRs obtained and can be used to estimate the attenuation uncertainty when the relationships proposed here are entered into seismic hazard assessment. This value is comparable to the intrinsic uncertainties of intensity estimates.

Seismic Hazard Assessment

The methodology used in most probabilistic seismic hazard analyses was originally proposed by Cornell (1968), and implemented in different computer codes (e.g., Algermissen *et al.*, 1976; McGuire, 1976; Bender and Perkins, 1987).

Computing seismic hazard consists of applying the total probability theorem,

$$\iiint f(M,\ D,\ T) fmfdft, \tag{20}$$

where *M, D*, and *T* are the random magnitude, distance, and time variables and *fm, fd*, and *ft* are their probability density functions.

The Cornell (1968) approach, in the Bender and Perkins (1987) formulation, computes the hazard at each site of the study region by discrete summation of the individual contributions from the mass center of the concentric circular sectors in which the SZs are subdivided. This distance is rigorously neither the epicentral distance nor that from the causative fault as spatially uniform seismicity is assumed in each SZ, but in practice it can be approximated to both.

Computation of the hazard maps was done over an approximately $0.1° \times 0.1°$ regular grid, using the software SEISRISK III (Bender and Perkins, 1987). The PGA is given in gravitational acceleration; the intensity maps are expressed in the MSK scale. Soft boundaries of variable width (Fig. 6) have been applied. All results are for a 475-year return period, which corresponds to a 90% nonexceedance probability in 50 years. This is a standard reference value in seismic design for ordinary buildings. In order to reduce the inevitable uncertainties introduced by the choice of the attenuation relations, the logic-tree methodology has been applied to the PGA results. Figure 14 illustrates the structure of the logic tree used to obtain the hazard curves (see the example of Santiago de Cuba), taking into account four attenuation relations (three for PGA and one for intensity transformed into PGA).

Hazard Results in PGA

The PGA results for a 475-year return period are presented in Figures 15 and 16; they refer respectively to the PGA mean value and to that computed taking into account the σ of the attenuation relation. The results obtained are considered to be robust for Cuba, Jamaica, and Hispaniola, with the exception of its easternmost sector, where the seismicity of SZs not considered in the present zonation could influence the hazard estimates. The most hazardous areas are consistent in all maps and depend on the seismogenic zonation used. In fact, the previous discussion of seismicity data has clearly pointed out that the earthquakes are concentrated along the southern coast of Cuba (OFZ) and eastward along the northern coast of Hispaniola (SFZ).

The first map uses the Ambraseys (1995) attenuation

Table 6

Earthquakes Selected for the Calibration of the Intensity Attenuation Relations

SZ	Date (yyyy mm dd)	I_{max}	I_o	Latitude (°N)	Longitude (°W)	N_f	N_s
5	1914 08 25	VII	VIII	21.22	76.17	43	54
8	1880 01 23	VIII	VIII	22.70	83.00	82	105
11	1982 12 16	VI	VI–VII	22.60	81.40	134	178
14	1939 08 15	VII	VII	22.51	79.58	42	56
15	1953 01 01	VI	VI	22.15	78.60	54	81
16	1974 04 08	VI	VI–VII	21.82	77.10	63	63
19	1962 07 19	VI	VI	20.52	77.20	13	17
20	1985 09 01	V	V–VI	19.86	75.39	54	65
22	1943 07 30	VI	VI	21.85	80.10	31	39
28	1992 05 25	VII	VIII	19.93	77.51	111	132
29	1932 02 03	VIII	IX	19.50	75.50	64	85
30	1947 08 07	VII	VIII	19.75	75.70	32	41

The SZ code refers to Figure 6; I_0 and coordinates derive from our elaborations. N_f is the number of intensity points with $I_s \geq$ II MSK, N_s is the number of intensity points where the uncertain data are counted twice because they are subdivided into other possible intensity classes.

Table 7

Coefficients of the Attenuation Relations According to the Different Selected Models

Model	Grandori *et al.* (1987)			Berardi *et al.* (1994)		Blake (1941)		von Kovesligethy (1907)		
Date (yyyy mm dd)	ψ	ψ_0	D_0	α	β	a	h	k	h	m
1914 08 25	2.140	1.753	12.987	**−1.65**	**0.802**	3.012	19.209	3.0	19.18	0.0006
1880 01 23	**1.655**	**1.491**	**9.112**	−2.616	1.277	4.311	16.968	3.0	13.018	7.0
1982 12 16	3.359	0.182	11.865	−3.126	1.69	4.68	11.132	**4.01**	**10.04**	**0.0007**
1939 08 15	**2.13**	**1.038**	**11.796**	−2.582	1.202	3.805	16.835	3.0	14.21	4.00
1953 01 01	1.445	2.305	6.766	**−2.507**	**1.278**	4.50	17.211	3.0	14.104	1.20
1974 04 08	1.528	2.848	2.645	−2.421	1.591	**3.997**	**7.039**	3.0	5.831	0.0014
1962 07 19				**−1.968**	**0.916**	2.965	17.762	3.0	17.482	0.0008
1985 09 01				−2.273	0.934	3.563	27.11	**3.0**	**24.48**	**0.002**
1943 07 30	1.233	3.336	6.547	**−2.469**	**1.198**	4.525	20.645	3.0	17.654	0.001
1992 05 25	**1.046**	**7.458**	**7.122**	−4.759	1.42	8.839	86.48	3.0	48.86	0.001
1932 02 03	1.288	1.466	18.974	**−4.149**	**1.421**	6.689	48.586	3.0	28.053	0.0089
1947 08 07	1.134	6.168	5.928	**−3.783**	**1.348**	6.391	45.84	3.0	29.795	0.001
Mean				**−0.206**	**1.112**	1.790	3.080			

relation (Fig. 15a). It shows the highest PGA values (larger than 0.25g) along the northern coast of Hispaniola, followed by those offshore the coast of Santiago de Cuba (larger than 0.20g). Additional hazard is located along the southern part of Hispaniola, along both coasts of Jamaica, and in two sectors of northern Cuba (Pinar del Rio and Villa Clara provinces, respectively, to the west and east).

The PGA values obtained using the Quijada *et al.* (1993) attenuation relation (Fig. 15b) are lower than those obtained with the Ambraseys (1995) relation. The maximum PGA (larger than 0.15g) is located along the northern coast of Hispaniola and offshore the Santiago de Cuba coast; values between 0.10g and 0.15g can be seen offshore Villa Clara and in the Pinar del Río region.

Even higher PGA values are obtained when the Joyner and Boore (1981) attenuation relation is considered (Fig. 15c), but exactly the same areas emphasized by the Ambraseys (1995) relation map stand out. Northern Hispaniola exceeds 0.40g, and the same value is expected offshore Santiago de Cuba. In addition to the seismic spots previously seen, high values also appear in the Camagüey Province and south of Cienfuegos.

Results increase notably when the attenuation σ is taken into account. The map from the Ambraseys (1995) attenuation relation (Fig. 16a) is rather similar to that without σ (Fig. 15a) and shows that high values (larger than 0.30g) are found in southern Cuba, near Santiago de Cuba, but all southeastern Cuba shows PGA values from 0.20g to 0.30g. In western Cuba, the PGA values do not exceed 0.25g (between 0.10g and 0.20g in Havana), and in central Cuba they are under 0.10g in some regions. The most seismic area is located east of Cuba along the northern coast of Hispaniola.

A different pattern is shown by the map obtained with the Quijada *et al.* (1993) attenuation relation (Fig. 16b) because it gives higher PGA values at greater distances (Fig. 9). The maximum values (larger than 0.40g) are located offshore Santiago de Cuba and along the northern coast of Hispaniola, while areas with values larger than 0.20g now ap-

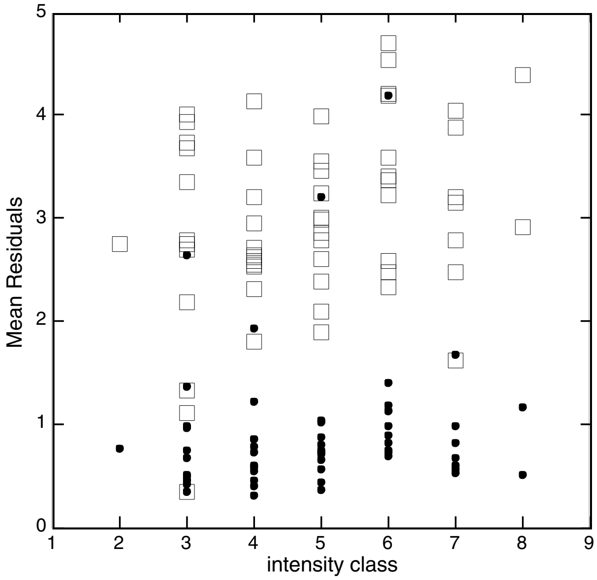

Figure 13. Mean residuals (MRs) for the 12 representative earthquakes: small dots indicate the MR values obtained using the best fitting attenuation relationship (type and coefficients enhanced in bold, in Table 7), while the open squares are the MR values obtained considering the average attenuation relationship.

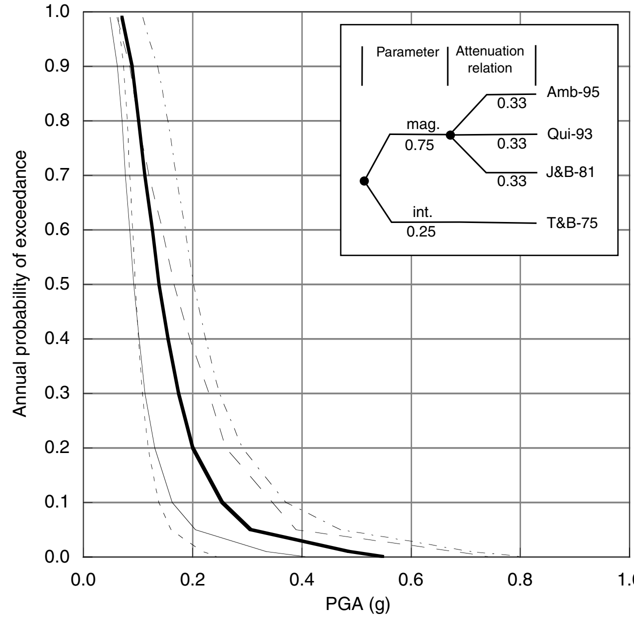

Figure 14. Seismic hazard curves (annual exceedence probability) for Santiago de Cuba according to different attenuation relations: thin solid line, Ambraseys (1995) (Amb-95); dotted line, Quijada *et al.* (1993) (Qui-93); dot-dashed line, Joyner and Boore (1981) (J&B-81); dashed line, differentiated intensity attenuation relations (intensity values converted into PGA values by the Trifunac and Brady [1975] relation) (T&B-75); thick solid line, final estimate (average value of the previous estimates). Two branches appear for seismicity because the magnitude and intensity rates were computed from the respective values in the catalog.

pear along both the northern and the southern Cuban coasts and in the western region (including Havana). The northern coast of Jamaica shows a limited area with values larger than 0.30*g*.

The map from the Joyner and Boore (1981) attenuation relation (Fig. 16c) reflects the pattern of the one obtained by the Ambraseys (1995) relations. The maximum values, in the Santiago de Cuba region and along the northern coast of Hispaniola, now exceed 0.80*g*.

Hazard Results in Macroseismic Intensity

The computation of intensity seismic hazard maps using many attenuation relationships does not differ from the ones for PGA, except that individual source contributions have to be separately calculated and added. Figure 17a shows the macroseismic intensity not expected to be exceeded at a 90% probability level in 50 years for the whole region, using the different intensity attenuation relationships previously described. From this picture we see that most of Cuba exhibits moderate intensity (V–VI MSK), with the highest values (VIII MSK) along its southern coast. Intensities around VII MSK are expected to affect a narrow strip along the eastern coast and the area of Pinar del Rio. At a wider scale, values close to IX MSK are expected along the northern coast of Hispaniola and intensity VIII MSK throughout Jamaica and almost all of Hispaniola.

The results obtained using only the average attenuation relationship are shown in Figure 17b. The relevance of this map is that it is obtained by the use of a single attenuation relation and can be compared with the previous one to pinpoint the main differences. This average map is similar to that of Figure 17a, except the southern coast of Cuba, where intensity VIII MSK is expected, is much smaller and is limited to a narrow strip along the coast. Consequently, the central part of the island also shows slightly lower values. No remarkable differences can be seen outside Cuba, as a mean attenuation relation was used in both maps.

It is worth mentioning that the results shown are mean values, and they do not take into consideration the attenuation uncertainty, as is usually done for PGA maps. One intensity unit of uncertainty can be considered, and in this case the expected shakings would be more severe on Cuba.

Comparing the present results (Fig. 17a) with those obtained by Rodriguez *et al.* (1997), our area of maximum intensity is larger and covers the whole southern coast of Cuba, instead of only the easternmost part as in the Rodriguez *et al.* (1997) map. Both maps show similar values with the exception of the Pinar del Rio area, where our area of intensity VII MSK is larger than that of Rodriguez *et al.* (1997). The values of Rodriguez *et al.* (1997) in the central part of the island are slightly higher than those we obtained.

The intensity estimates (Fig. 17a) have been converted

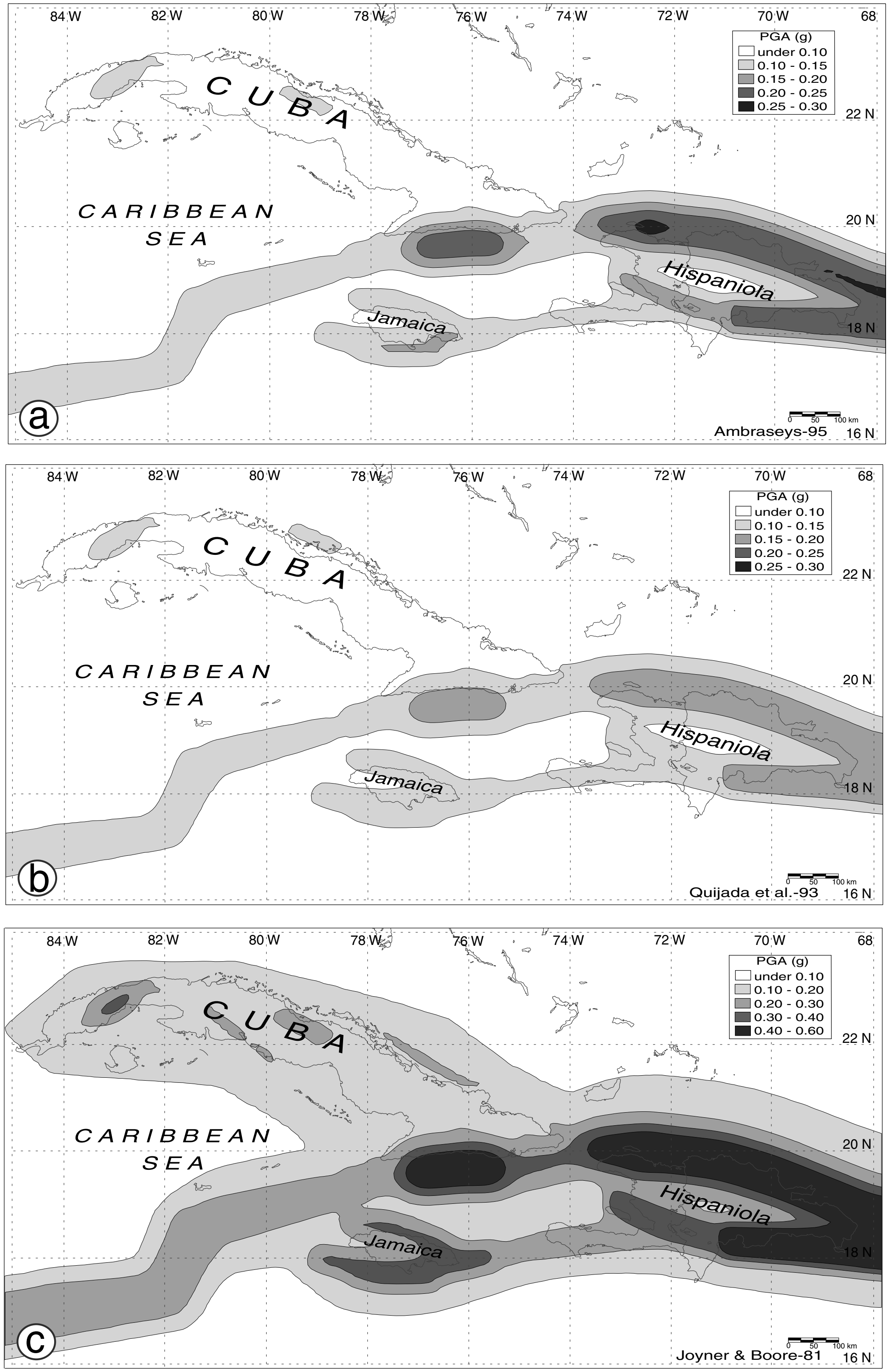

Figure 15. Horizontal PGA (in gravitational acceleration) with a 475-year return period considering (a) the Ambraseys (1995), (b) the Quijada *et al.* (1993), and (c) Joyner and Boore (1981) attenuation relations for average soil without σ.

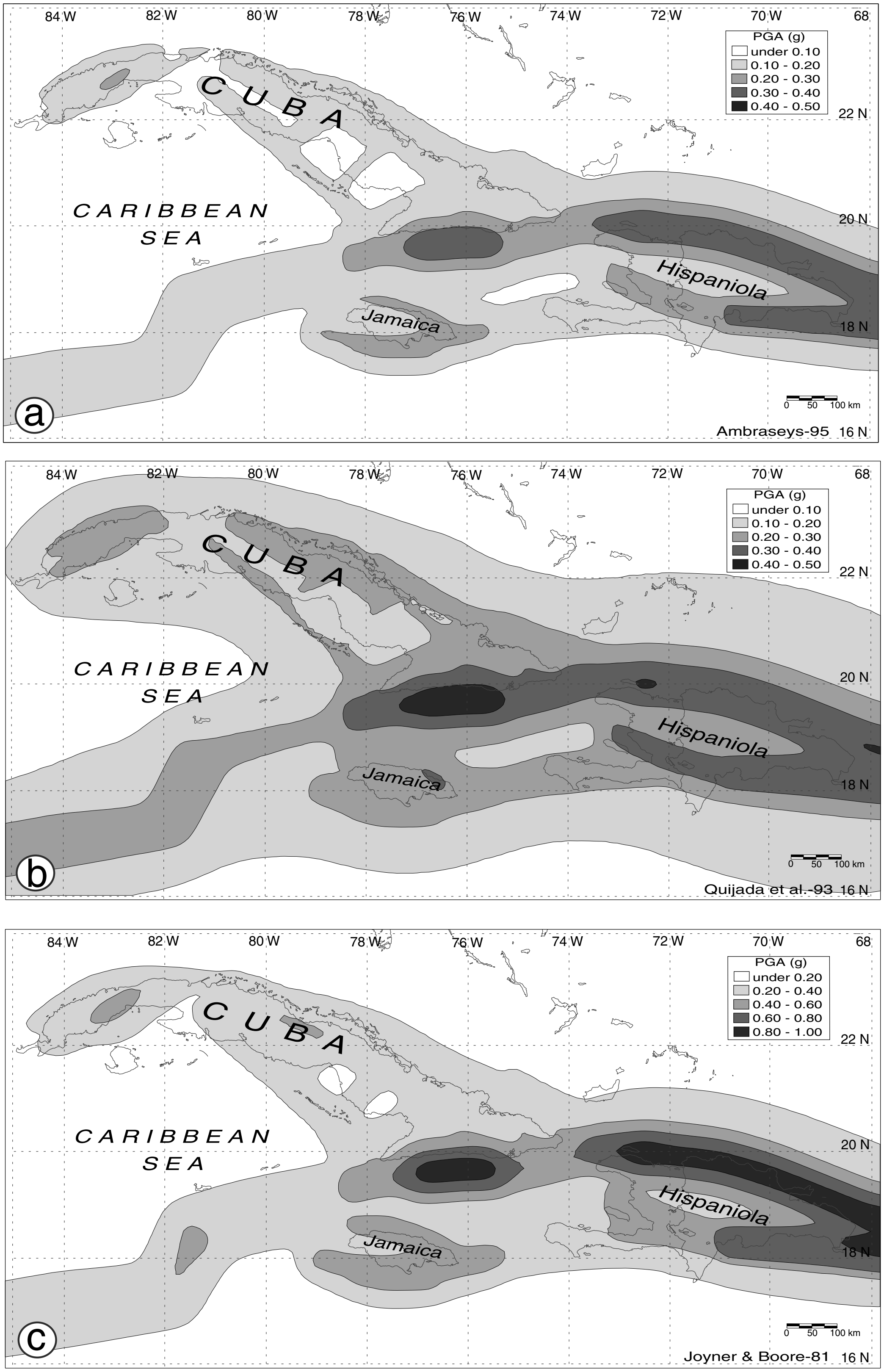

Figure 16. Horizontal PGA (in gravitational acceleration) with a 475-year return period considering (a) the Ambraseys (1995), (b) the Quijada *et al.* (1993), and (c) Joyner and Boore (1981) attenuation relations for average soil with σ.

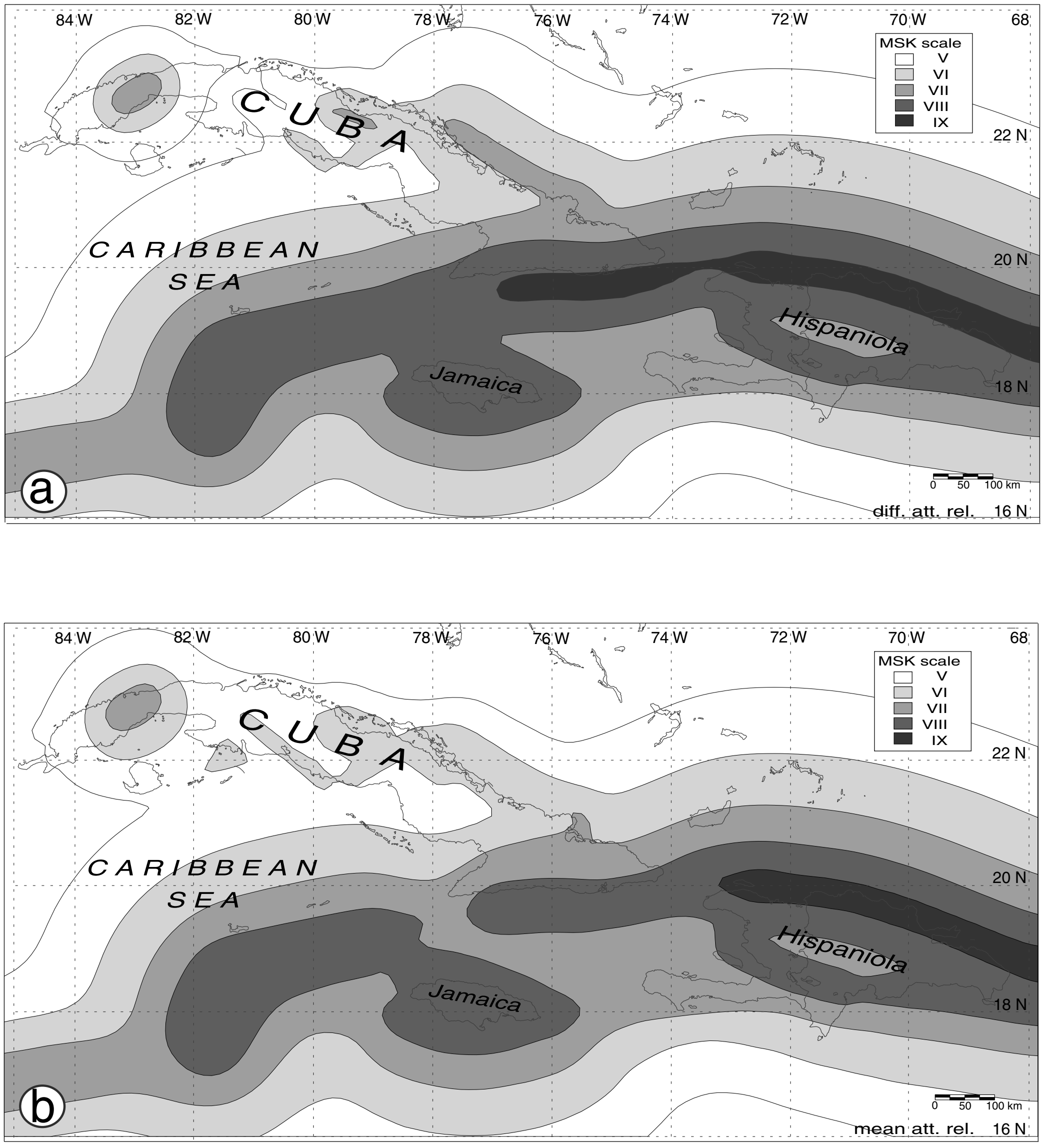

Figure 17. Macroseismic intensity with a 475-year return period using (a) different attenuation relations and (b) the average attenuation relation. No σ in the attenuation has been considered. Half degrees are rounded up in the graphical representation.

into PGA values (Fig. 18) by the Trifunac and Brady (1975) relation, the relation most used in previous Cuban studies, for a direct comparison with the direct PGA estimates (Fig. 15). The PGA from the intensity map (Fig. 18) shows obvious similarities to the direct PGA maps (Fig. 15), with the maximum hazard along the northern coast of Hispaniola and the southern coast of Cuba. The PGA values along the southern coast of Cuba do not differ much from those obtained considering the Joyner and Boore (1981) attenuation relation (Fig. 15c), but much lower hazard is expected on the rest of the Cuban territory.

Hazard Results Following the Logic-Tree Approach

Following a logic-tree approach (McGuire, 1977; McGuire and Shedlock, 1981; Kulkarni *et al.*, 1984; Coppersmith and Youngs, 1986), a map has been computed averaging the values of the individual maps presented before. This map can be considered more robust as it is less dependent on the specific choice of attenuation.

All the PGA results (Figs. 15 and 18) were merged with the same weight (0.25) and an average hazard curve obtained. This hazard curve is reported here only for Santiago de Cuba (Fig. 14): it can be seen that the results considering the Ambraseys (1995) and the Quijada *et al.* (1993) relations are similar, while those considering the Joyner and Boore (1981), as well as those considering intensity, are higher.

Figure 19 shows the average PGA values for the whole study region. It is interesting to note that some peculiarities of the previous maps are reflected on this final map as well. For example, in southern Cuba the influence of the Bartlett–

Cayman fault (OFZ) is clear all along the southern coast of the island, where the PGA reaches 0.30*g* and decreases rapidly to the north. This high hazard strip continues eastward along the northern coast of Hispaniola, with values only slightly larger. In central Cuba, the northern coast, especially the Pinar del Rio region, represents the more hazardous area, with PGA values larger than 0.10*g*.

Comparing the results of our final map (Fig. 19) to those obtained by Rodriguez *et al.* (1997), similar values (larger than 0.30*g*) are encountered along the southern coast of Cuba, but our maximum is shifted toward Santiago. The high spots around the Guantanamo and Pinar del Rio regions do not appear so evidently in the Rodriguez *et al.* (1997) map, and they do not appear in the Shepherd *et al.* (1997) map either, but this last map has the maximum for Cuba (PGA larger than 0.24*g*) exactly around Santiago, where our maximum is also located.

The GSHAP map for the Caribbean (Shedlock, 1999) refers to rock and shows PGAs larger than 0.32*g* in the Santiago de Cuba area; this value is lower than those displayed in Figure 16 (with the exception of the map obtained by the Ambraseys [1995] attenuation relation, which is similar) because our results refer to an average soil. The westernmost part of the island is characterized by very low values in the

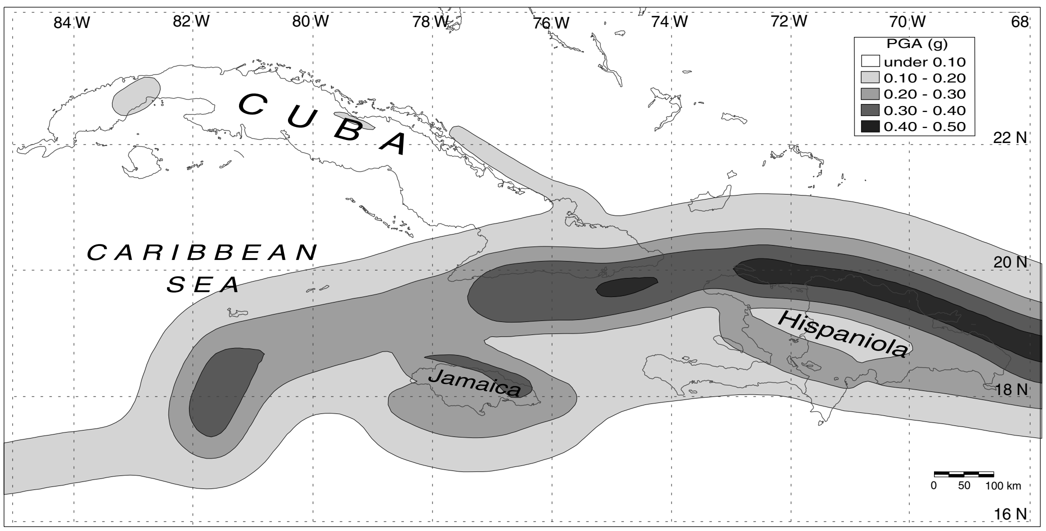

Figure 18. Horizontal PGA (in gravitational acceleration) with a 475-year return period obtained transforming the intensity values (Fig. 17a) into PGA values by the Trifunac and Brady (1975) relation.

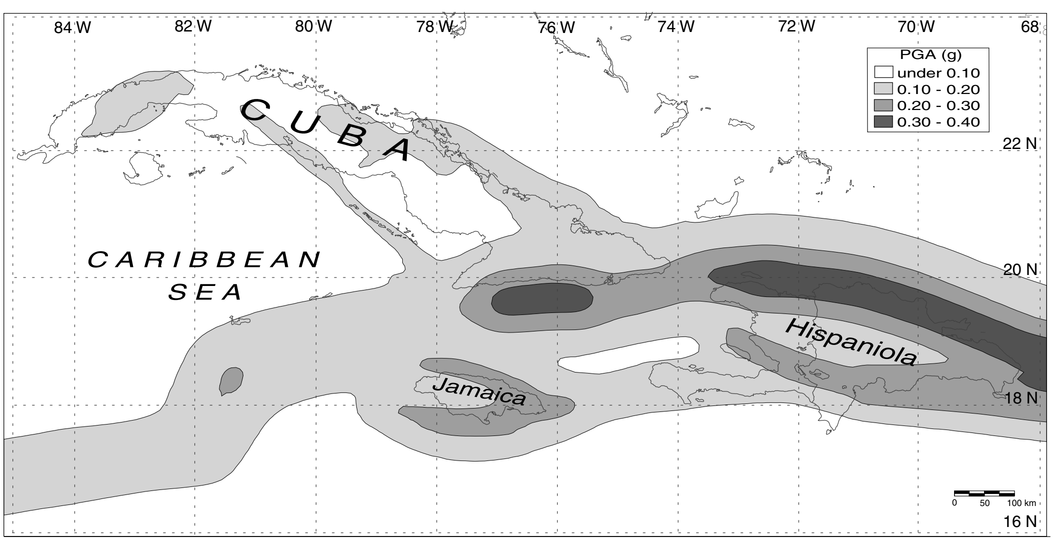

Figure 19. Average horizontal PGA (in gravitational acceleration) with a 475-year return period for average soil, following the logic-tree approach. No σ in the attenuation has been considered.

GSHAP map (Shedlock, 1999). All our results, in contrast, show higher PGA values along the northern and southern coasts and the seismic spot in the Pinar del Rio region, caused by the influence of SZ8 (Fig. 6). A direct comparison with our final results cannot be made, as our map in Figure 19 does not consider the aleatory uncertainty of attenuation, while the GSHAP map (Shedlock, 1999) does.

The seismic hazard map for Latin America and the Caribbean prepared by Tanner and Shepherd (1997) shows only that the maximum PGA in Cuba is located offshore Santiago (values larger than 0.25*g* on rock), with no further details.

Conclusions

The present study offers a new, comprehensive view of seismic hazard on Cuban territory, using the most recent international investigations on the subject. In the present study, some aspects of seismic hazard calculation have been treated specifically, as follows:

- A data set, where each earthquake is characterized by several entries coming from different sources, has been created for systematic storage and analysis. The earthquake catalog of Cuba and neighboring areas is hazard oriented, where a specific processing method (magnitude values, filtering techniques, location and epicentral intensity of offshore events) was applied to the data set.
- All the available macroseismic data for Cuba were analyzed to investigate the problem of intensity attenuation relationships. Four models were considered, including the von Kovesligethy (1907) relation that has been traditionally used in Cuba. As the seismic hazard results depend critically on the chosen attenuation relation, our choice was to prefer different relations for the different SZs, so that the most severe event that occurred in the past is taken as representative of the attenuation properties.
- Three different PGA attenuation relationships from the literature have been considered, as a local attenuation relation is not available for the Caribbean region. Hazard estimates are referred to an average soil type, as the association of simplified local conditions (e.g., rock, stiff, and soft soil) is not currently feasible. Moreover, the use of a logic-tree approach, where estimates in intensity are also included, automatically excludes any possible evaluation of local effects. The final hazard map has been computed by weighting the individual results obtained by the application of the cited PGA relations and those of the hazard map in terms of macroseismic intensity. In such a way, the importance of the choice of the attenuation relation is minimized.
- The final results, both in terms of PGA and intensity, indicate a high hazard along the southern coast of Cuba, where Santiago de Cuba is located. The rest of the island is characterized by moderate values that do not represent the possibility of very severe damage at the specified annual probability level.

Acknowledgments

This research has been developed in the framework of the ICTP Programme for Training and Research in Italian Laboratories of the International Centre for Theoretical Physics, Miramare, Trieste, Italy. Many thanks are due to the associate editor of the *Bulletin*, Ivan Wong, URS Corporation Oakland, Charles Mueller, U.S. Geological Survey, Denver, and an anonymous reviewer for their very useful comments and improvements and to Muzio Bobbio, OGS Trieste, for his cooperation and support.

References

Algermissen, S. T., D. M. Perkins, W. Isherwood, D. Gordon, G. Reagor, and C. Howard (1976). Seismic risk evaluation of the Balkan region, in *Proc. of the Seminar on Seismic Zoning Maps*, V. Karnik and C. Radu (Editors), Vol. 2, Unesco, Skopje, 172–240.

Alvarez, L. (1995). SACUDIDA: *versión 2.0—Un Programa para la Estimación de la Peligrosidad Sísmica*, Editorial Academia, La Habana, Cuba, 1–59.

Alvarez, L., and V. I. Bune (1977). Evaluating the seismic hazard for the southeastern part of Cuba, *Izv. Akad. Nauk SSSR Fiz. Zemli* **10,** 54–67 (in Russian).

Alvarez, L., and V. I. Bune (1985a). Seismic hazard in eastern Cuba, *Izv. Earth Phys.* **21,** 733–741.

Alvarez, L., and V. I. Bune (1985b). A computer program for seismic hazard estimation, in *Proc. 3rd Int. Symp. Analysis of Seismicity and Seismic Risk*, Czechoslovak Academy of Sciences, Prague, 432–439.

Alvarez, L., and T. Chuy (1985). Isoseismal model for Greater Antilles, in *Proc. 3rd Int. Symp. Analysis of Seismicity and Seismic Risk*, Czechoslovak Academy of Sciences, Prague, 134–141.

Alvarez, L., R. S. Mijailova, E. O. Vorobiova, T. Chuy, G. N. Zhakirzhanova, E. R. Perez, L. M. Rodionova, H. Alvarez, and K. M. Mirzoev (1990). Terremotos de Cuba y áreas aledañas, Internal report, Fondos del CENAIS, 1–78.

Alvarez, L., T. Chuy, and M. Cotilla (1991). Peligrosidad sísmica de Cuba: una aproximación a la regionalización sísmica del territorio nacional, *Rev. Geofís.* **35,** 125–150.

Ambraseys, N. N. (1995). Reappraisal of the prediction of ground accelerations in Europe: EAEE Working Group report, in *10th European Conf. on Earthquake Engineering*, G. Duma (Editor), Balkema, Rotterdam, The Netherlands, 3041–3048.

Belousov, T. P., V. N. Krestnikov, and N. V. Shebalin (1983). Seismic source zones delimitation and estimation of maximum magnitudes from Central Cuba, in *Research of the Seismicity of Low Activity Seismic Zones* (Central Cuba), Nauka, Moscow, 81–85.

Bender, B., and D. M. Perkins (1987). SEISRISK III: a computer program for seismic hazard estimation, *U.S. Geol. Surv. Bull. 1772*, Denver, Colorado, 1–48.

Berardi, R., L. Magri, M. Mucciarelli, C. Petrungaro, and L. Zanetti (1994). Mappe di sismicità per l'area italiana, ENEL, Roma, 1–60.

Blake, A. (1941). On the estimation of focal depth from macroseismic data, *Bull. Seism. Soc. Am.* **31,** 225–231.

British Association Seismology Committee (1918). *Bulletin 1913–1915*, Earthquake Observatory, Shide, United Kingdom.

British Association Seismology Committee (1919). *The Large Earthquakes of 1916*, University Observatory, Oxford, United Kingdom.

British Association Seismology Committee (1921). *Bulletin 1917*, University Observatory, Oxford, United Kingdom.

Calais, E., B. Mercier, and M. de Lepinay (1991). From transtention to transpression along the northern Caribbean plate boundary of Cuba: implications for the recent motion of the Caribbean plate, *Tectonophysics* **186,** 329–350.

Chuy, T. (1999). Macrosísmica de Cuba y su aplicación en los estimados de peligrosidad sísmica y microzonación sísmica, *Ph.D. Thesis*, CENAIS, Santiago de Cuba, Cuba, 1–95.

Chuy, T., and M. Rodriguez (1980). La actividad sísmica de Cuba por datos históricos, *Investigaciones Sismológicas en Cuba* **1,** 5–17.

Chuy, T., B. Gonzalez, and L. Alvarez (1983). Sobre la peligrosidad sísmica en Cuba, *Investigaciones Sismológicas en Cuba* **4,** 37–52.

Chuy, T., L. Alvarez, J. Zapata, and B. Gonzalez. (1992). Investigaciones sismológicas complejas para el Complejo Hidroenergético Toa-Duaba, Reporte de Investigación, Fondos del CENAIS, 1–745.

Chuy, T., and L. Alvarez (1995). Seismic hazard map of Cuba for the new building code of the Republic of Cuba, Ministry of Construction, Havana, 1–21, scale 1:1,000,000 (in Spanish).

Cornell, C. A. (1968). Engineering seismic risk analysis, *Bull. Seism. Soc. Am.* **58,** 1583–1606.

Cotilla, M. O. (1998). An overview on the seismicity of Cuba, *J. Seism.* **2,** 323–335.

Cotilla, M., and L. Alvarez (2001). Seismogenic regularities of the Cuban western seismotectonic unit, *Geol. J. Chile* **28,** 3–24 (in Spanish).

Cotilla, M., P. Bankwitz, A. Franzke, L. Alvarez, E. Gonzalez, J. Diaz, G. Gruenthal, J. Pilarski, and F. Arteaga (1991). Mapa sismotectónico de Cuba Escala 1:1000000, *Comunicaciones Científicas sobre Geofísica y Astronomía* **23,** 1–49, 1er anexo.

Cuevas, J. L. (1994). Estudios de isostasia en Cuba: una caracterización y delimitación de zonas potencialmente sísmicas, *Bol. Geol. Minero* **109,** 265–278.

Coppersmith, K. J., and R. R. Youngs (1986). Capturing uncertainty in probabilistic seismic hazard assessments within intraplate environments, in *Proc. of the 3rd U.S. National Conference on Earthquake Engineering*, 24–28 August 1986, Charleston, South Carolina, Vol. 1, 301–312.

Dimaté, C., L. Drake, H. Yepez, L. Ocola, H. Rendon, G. Gruenthal, and D. Giardini (1999). Seismic hazard assessment of the Northern Andes (PILOTO Project), *Ann. Geofis.* **42,** 1039–1055.

Fedotov, S. A., and L. S. Shumilina (1971). Seismic hazard of Kamchatka, *Izv. Akad. Nauk S.S.S.R. Fiz. Zemli* **9,** 3–15 (in Russian).

Garcia, J. A. (2001). Seismic hazard assessment for Cuba and the surrounding area, Research Report, ICTP, Trieste, Italy, 1–80.

Gardner, J. K. and L. Knopoff (1974). Is the sequence of earthquakes in southern California, with aftershocks removed, Poissonian? *Bull. Seism. Soc. Am.* **64,** 1363–1367.

Giardini D. (1999). The Global Seismic Hazard Assessment Program (GSHAP): 1992/1999, *Ann. Geofis.* **42,** 957–974.

Giardini, D., and P. Basham (1993). The Global Seismic Hazard Assessment Program (GSHAP), *Ann. Geofis.* **36,** 3–13.

Gonzalez, B. E., T. Chuy, L. Alvarez, and M. F. Rubio (1993). Estudios sismológicos complejos de Cuba centro oriental para el emplazamiento de objetivos nucleares, Reporte de Investigación, Fondos del CENAIS, 1–357.

Gabrielov, A. M., O. E. Dmitrieva, V. I. Keilis-borok, V. G. Kossobokov, I. V. Kutznetsov, T. A. Levshina, K. M. Mirzoev, G. M. Molchan, S. Kh. Negmatullaev, V. F. Pisarenko, A. G. Prozorov, W. Rinheart, I. M. Rotwain, P. N. Shebalin, M. G. Shnirman, and S. Yu. Schreider (1986). Algorithms of long-term earthquakes' prediction, Software and Data Handling, International School for Research Oriented to Earthquake Prediction-algorithms, Lima, Perù, 1–61.

Grandori, G., F. Perotti, and A. Tagliani (1987). On the attenuation of macroseismic intensity with epicentral distance, in *Ground Motion and Engineering Seismology*, A. S. Cakmak (Editor), Elsevier, Amsterdam, 581–594.

International Seismological Summary (1918–1963). The International Seismological Summmary 1918–1963, University Observatory/I.S.C., Oxford.

International Seismological Centre (ISC) (1964–1995). *Regional Catalogue of Earthquakes, 1964–1995*, Edinburgh.

Iturralde-Vinent, M. (1994). Cuban geology: a new plate tectonic synthesis, *J. Petrol. Geol.* **17,** 39–70.

Iturralde-Vinent, M. (Editor) (1996). Ofiolitas y arcos volcánicos de Cuba, First Contribution of IGCP Project 364, Geological Correlation of Ophiolites and Volcanic Arc Terrains in the Circum Caribbean Region, Miami, U.S.A, 1–265.

Joyner, W. B., and D. M. Boore (1981). Peak horizontal acceleration and velocity from strong-motion records including records from the 1979 Imperial Valley, California, earthquake, *Bull. Seism. Soc. Am.* **71,** 2011–2038.

Kulkarni, R. B., R. R. Youngs, and K. J. Coppersmith (1984). Assessment of confidence intervals for results of seismic hazard analysis, in *Proc. of the 8th World Conference on Earthquake Engineering*, 21–28 July 1984, San Francisco, Vol. 1, 263–270.

Lundgren, P. R., and R. M. Russo (1996). Finite element modeling of crustal deformation in the North America-Caribbean plate boundary zone, *J. Geophys. Res.* **101,** 11,317–11,327.

Mann, P., K. Burke, and T. Matumoto (1984). Neotectonics of Hispaniola: plate motion, sedimentation, and seismicity at a restraining bend, *Earth Planet. Sci. Lett.* **70,** 311–324.

Mann, P., F. W. Tailor, R. L. Edwars, and T. L. Ku (1995). Actively evolving microplate formation by oblique collision and sideways motions along strike-slip faults: an example from the northeastern Caribbean plate margin, *Tectonophysics* **246,** 1–69.

McGuire, R. K. (1976). Fortran computer program for seismic risk analysis, *U.S. Geol. Surv. Open-File Rept. 76-67*, 1–92.

McGuire, R. K. (1977). Effects of uncertainties in seismicity on estimates of seismic hazard for the east coast of the United States, *Bull. Seism. Soc. Am.* **67,** 827–848.

McGuire, R. K., and K. M. Shedlock (1981). Statistical uncertainties in seismic hazard evaluations in the United States, *Bull. Seism. Soc. Am.* **71,** 1287–1308.

Meletti, C., E. Patacca, and P. Scandone (2000). Construction of a seismotectonic model: the case of Italy, *Pure Appl. Geophys.* **157,** 11–35.

Moreno, B., M. Grandison, and K. Atakan (2002). Crustal velocity model along the southern Cuban margin: implications for the tectonic regime at an active plate boundary, *Geophys. J. Int.* **151,** 632–645.

Murphy, J. R., and L. J. O'Brien (1977). The correlation of peak ground acceleration amplitude with seismic intensity and other physical parameters, *Bull. Seism. Soc. Am.* **67,** 877–915.

Muir-Wood, R. (1993). From global seismotectonics to global seismic hazard, *Ann. Geofís.* **36,** 153–168.

Nuevo Atlas Nacional de Cuba (1989). Sección III: Características geofísicas, Instituto de Geografía de la Academia de Ciencias de Cuba, Instituto Cubano de Geodesia y Cartografía y Instituto de Geografía Nacional (Madrid, España), II.3.3.

Orbera, L., B. Gonzalez, T. Chuy, and J. Oro (1990). Investigación sísmica en la región de emplazamiento del Centro de Investigaciones Nucleares, Reporte de Investigación, Fondos del CENAIS y la SEAN, 1–344.

Orbera, L., J. Rodríguez, B. Pena, A. Arias, M. Marqueti, and T. Lombardero (1989). Estudio sismotectónico para el emplazamiento del Complejo Hidroenergético Toa-Duaba, Reporte de Investigación, Fondos del E.I.P.I.B., MINBAS, 1–180.

Peruzza, L. (1995). Macroseismic intensity versus distance: constraints to the attenuation model, in *Soil Dynamics and Earthquake Engineering VII*, A. S. Cakmak and C. A. Brebbia (Editors), Computational Mechanics Publications, Southampton, England, 215–222.

Peruzza, L. (1996). Attenuating intensities, *Ann. di Geofis.* **39,** 1079–1093.

Peruzza, L. (2000). Macroseismic attenuation relationships of Italian earthquakes for seismic hazard assessment purposes, *Boll. Geof. Teor. Appl.* **41,** 31–48.

Puscharovsky, Y., A. Mossakovsky, G. Nekrasov, S. Sokolov, and M. Iturralde-Vinent (1989). Tectonics of the Republic of Cuba: explanatory note to the tectonic map of Cuba, scale 1: 500,000, Editor Nauka, Moscow, 1–77 (in Russian).

Quijada, P., E. Gajardo, M. Franke, M. Kozuch, and J. Grases. (1993). Analisis de amenaza sismica de Venezuela para el nuevo mapa de zonificacion con fines de ingenieraia, in *Memorias del Octavo Seminario Latinoamericano de Ingenieraia Sismo-Resistente*, Merida.

Rautian, T. G. (1964). On the determinantion of earthquake energy for distances lower than 3000 km, *Trudi Instituta Fizika Zemli* **32,** 88–93 (in Russian).

Rebez, A., and D. Slejko (2000). Sensitivity analysis on the input parameters in probabilistic seismic hazard assessment, *Soil Dyn. Earthquake Eng.* **20,** 341–351.

Reiter, L. (1990). Earthquake hazard analysis: issues and insights, Columbia University Press, New York, 1–252.

Richter, C. F. (1958). *Elementary Seismology*, Freeman, San Francisco.

Riznichenko, Yu. V. (Editor) (1979). *Seismic Hazard in the Territory of the U.S.S.R.*, Nauka, Moscow, 1–184 (in Russian).

Rodriguez Farrat, M., L. Alvarez, and J. Garcia (1997). Estimaciones probabilísticas de la peligrosidad sísmica en Cuba, *Rev. Geofís.* **47,** 46–77.

Rosencrantz, E., M. I. Ross, and J. G. Sclater (1988). Age and spreading history of the Cayman trough as determination from depth heat flow, and magnetic anomalies, *J. Geophys. Res.* **93,** 2141–2157.

Rosencrantz, E., and P. Mann (1991). SeaMARC II mapping of transform faults in the Cayman Trough, Caribbean Sea, *Geology* **19,** 690–693.

Rubio, M. (1985). The assessment of seismic hazard for the Republic of Cuba, in *Proc. 3rd Int. Symp. Analysis of Seismicity and Seismic Risk*, Czechoslovak Academy of Sciences, Prague, 424–431.

Russo, R. M., and A. Villaseñor (1995). The 1946 Hispaniola earthquakes and the tectonics of the North America–Caribbean plate boundary zone, northeastern Hispaniola, *J. Geophys. Res.* **100,** 6265–6280.

Servicio Sismológico Nacional (1964–1995). Boletines anuales de datos sismologicos, Fondos del CENAIS.

Shedlock, K. M. (1999). Seismic hazard map of North and Central America and the Caribbean, *Ann. Geofis.* **42,** 977–999.

Shedlock, K. M., and J. G. Tanner (1999). Seismic hazard map of the western hemisphere, *Ann. Geofis.* **42,** 1199–1214.

Shepherd, J. B., J. G. Tanner, C. M. McQueen, and L. L. Lynch (1997). Seismic hazard in Latin America and the Caribbean, in *Seismic Hazard Maps for the Caribbean*, IRDC, Ottawa, Vol. 5, 15.

Slejko, D., L. Peruzza, and A. Rebez (1998). Seismic hazard maps of Italy, *Ann. Geofis.* **41,** 183–214.

Slejko, D., R. Camassi, I. Cecic, D. Herak, M. Herak, S. Kociu, V. Kouskouna, J. Lapajne, K. Makropoulos, C. Meletti, B. Muco, C. Papaioannou, L. Peruzza, A. Rebez, P. Scandone, E. Sulstarova, N. Voulgaris, M. Zivcic, and P. Zupancic (1999). Seismic hazard assessment for Adria, *Ann. Geofis.* **42,** 1085–1107.

Speed, R. C., and D. K. Larue (1991). Extension and transtension in the plate boundary zone of northeastern Caribbean, *Geophys. Res. Lett.* **18,** 573–576.

Sponheuer, W. (1960). Berachnungverfahren mit Schrittweiser Nahorung, in *Methoden zur Herdtiefen Bestimmung in der Makroseismic*, W. Sponheuer (Editor), Freiberger Forshungshefte C88, Akademie Verlag, Berlin, 16–32.

Stepp, J. C. (1972). Analysis of completeness of the earthquake sample in the Puget Sound area and its effect on statistical estimates of earthquake hazard, in *Proc. of the 1st Int. Conf. on Microzonazion*, Seattle, Vol. 2, 897–910.

Tanner J. G., and J. B. Shepherd (1997). Seismic hazard in Latin America and the Caribbean, in *Project Catalog and Seismic Hazard Maps*, IRDC, Ottawa, Vol. 1, 143.

Trifunac, M. D., and A. G. Brady (1975). On the correlation of seismic intensity scales with the peaks of ground motion records, *Bull. Seism. Soc. Am.* **65,** 139–162.

Veneziano, D. C., A. Cornell, and T. O'Hara (1984). Historical method of seismic hazard analysis, Rep. NP-3428, Electric Power Research Institute, Palo Alto, California.

von Kovesligethy, R. (1907). Seismischer Stärkegrad und Intensität der Beben, *Gerlands Beitr. Geophys.* **8,** 363–366.

Centro Nacional de Investigaciones Sismológicas
Calle 212 No. 2906, e/29 y 31
La Coronela, La Habana, Cuba
(J.G., L.A.)

Istituto Nazionale di Oceanografia e di Geofisica Sperimentale
Borgo Grotta Gigante 42c
34010 Sgonico (Trieste), Italy
(D.S., L.P., A.R.)

Manuscript received 25 June 2002.